Title
Ribonucleotide Reductases: Structure, Chemistry, and Metabolism Suggest New Therapeutic Targets.

Journal
Annual review of biochemistry, 89(1)

ISSN
0066-4154

Authors
Greene, Brandon L
Kang, Gyunghoon
Cui, Chang
et al.

Publication Date
2020-06-01

DOI
10.1146/annurev-biochem-013118-111843

Peer reviewed

ANNUAL REVIEWS

Annual Review of Biochemistry

Ribonucleotide Reductases: Structure, Chemistry, and Metabolism Suggest New Therapeutic Targets

Brandon L. Greene,[1,2,3] Gyunghoon Kang,[2] Chang Cui,[2,3] Marina Bennati,[4,5] Daniel G. Nocera,[3] Catherine L. Drennan,[2,6,7] and JoAnne Stubbe[2,6]

[1]Department of Chemistry and Biochemistry, University of California, Santa Barbara, California 93106, USA

[2]Department of Chemistry, Massachusetts Institute of Technology, Cambridge, Massachusetts 02139, USA; email: stubbe@mit.edu

[3]Department of Chemistry and Chemical Biology, Harvard University, Cambridge, Massachusetts 02138, USA

[4]Max Planck Institute for Biophysical Chemistry, 37077 Göttingen, Germany

[5]Department of Chemistry, University of Göttingen, 37073 Göttingen, Germany

[6]Department of Biology, Massachusetts Institute of Technology, Cambridge, Massachusetts 02139, USA

[7]Howard Hughes Medical Institute, Massachusetts Institute of Technology, Cambridge, Massachusetts 02139, USA

Annu. Rev. Biochem. 2020. 89:45–75

The *Annual Review of Biochemistry* is online at biochem.annualreviews.org

https://doi.org/10.1146/annurev-biochem-013118-111843

Keywords

ribonucleotide reductases, structures, mechanisms, therapeutics

Abstract

Ribonucleotide reductases (RNRs) catalyze the de novo conversion of nucleotides to deoxynucleotides in all organisms, controlling their relative ratios and abundance. In doing so, they play an important role in fidelity of DNA replication and repair. RNRs' central role in nucleic acid metabolism has resulted in five therapeutics that inhibit human RNRs. In this review, we discuss the structural, dynamic, and mechanistic aspects of RNR activity and regulation, primarily for the human and *Escherichia coli* class Ia enzymes. The unusual radical-based organic chemistry of nucleotide reduction, the inorganic chemistry of the essential metallo-cofactor biosynthesis/maintenance, the transport of a radical over a long distance, and the dynamics of subunit interactions all present distinct entry points toward RNR inhibition that are relevant for drug discovery. We describe the current mechanistic understanding of small molecules that target different elements of RNR function, including downstream pathways that lead to cell cytotoxicity. We conclude by summarizing novel and emergent RNR targeting motifs for cancer and antibiotic therapeutics.

Contents

INTRODUCTION

The availability of adequate and balanced deoxynucleotide pools is essential for accurate DNA replication and repair and, consequently, for genome stability. Deoxynucleotides are supplied universally in all organisms by a de novo pathway catalyzed by ribonucleotide reductases (RNRs) that convert RNA building blocks to DNA building blocks (1–3). Deoxynucleotides can also be generated in an organism-, environment-, and disease-specific fashion by nucleoside (or nucleotide) salvage pathways (4). Our current understanding of the unique organic (5) and

RNR: ribonucleotide reductase

inorganic chemistry (6) of RNRs has been revealed, in part, by our understanding of clinically used therapeutics that target the universal radical-mediated nucleotide reduction mechanism and of the specific metallo-cofactor biosynthetic and repair pathways. An ensemble of studies led to the first structures of class I RNRs at low resolution (7–10) and, more recently, to high-resolution structures in trapped active and inhibited states (8, 11, 12). These recent studies suggest, in combination with inhibitors of specific signaling pathways downstream of RNR, that the time is right to revisit RNRs as a target for antibacterial, antiviral, as well as anticancer agents.

All RNRs catalyze the conversion of nucleoside 5′-diphosphates (NDPs) or triphosphates (NTPs) to deoxynucleotides (dNDP or dNTP) (**Figure 1*a***). The RNRs share a common active-site architecture located in subunit α that houses three essential cysteines (**Figure 1*b***) (13). Two cysteines (on the bottom face of the RNR) provide the reducing equivalents to make dNDPs, and the third cysteine (on the top face of the RNR) is transiently oxidized to a thiyl radical (–S•) that initiates NDP reduction (14). Distinct metallo-cofactors catalyze this oxidation (**Figure 1*c***), and they are the primary basis for RNR classification (Ia–e, II, III), although a recently discovered non-metallo-cofactor, 2,3-dihydroxy-phenylalanine radical (DOPA•), breaks this paradigm (15–17). This review focuses on the class I RNRs, which share a distinct mechanism by which a transient –S• is generated and whose formation requires a second subunit, β, that houses the cofactor oxidant (**Figure 1*c***) (18, 19).

α: the large subunit of RNR (80 kDa) that in active class Ia RNR is likely α2

–S•: thiyl radical

β: the small subunit of class Ia RNR (47 kDa) that is always β2

Radical transfer (RT): the reversible 35-Å pathway between Y_{122}• in β and C_{439} to be oxidized in α that involves multiple amino acid radical intermediates

Proton-coupled electron transfer (PCET): a central mechanism involved in oxidation/reduction chemistry in biology

Photosensitized RNR (photo-RNR): an α2β2 complex in which β is modified with a photooxidant that generates, with light, the Y_{356}•-β in the RT pathway; this method allows the uncoupling of conformational gating and measurement of the chemistry within α

Y•: tyrosyl radical, a one-electron-oxidized tyrosine with proton loss

Docking Model and Radical Transfer Pathway

In 1969, Reichard and colleagues discovered the class Ia *Escherichia coli* RNR and proposed that the active enzyme is an α2β2 complex (20, 21). However, not until 1994 was the X-ray structure of α2 reported, by Uhlin & Eklund (13) (**Figure 2*b***); this structure, together with their earlier structure of β2 (**Figure 2*a***) (19), led to a symmetrical docking model based on subunit shape complementarity (**Figure 2*c***) (13). This model guided experimentation until recently. A fascinating feature of the docking model is that the diferric-tyrosyl radical cofactor (Fe^{3+}_2-Y_{122}•) (**Figure 2*c***) in β is ~35 Å away from C_{439} (in *E. coli* numbering), which is oxidized in the α subunit. The turnover frequency for dNDP production (2–10 s^{-1}), together with the long distance between Y_{122}• and C_{439}, engenders a radical transfer (RT) pathway (7, 18): Y_{122}•[β] ⇌ [W_{48}[β]] ⇌ Y_{356}[β] to Y_{731}[α] ⇌ Y_{730}[α] ⇌ C_{439}[α] (**Figure 3**) (note that [W_{48}] involvement has not yet been demonstrated).

One or more rate-limiting physical steps mask both NDP reduction and RT chemistry. These processes are conformationally gated by proper substrate and effector binding to α2 and its association with β2 (22). The stable Y_{122}• in β2 is transiently reduced and reoxidized on each turnover, and RT through the pathway involves distinct proton-coupled electron transfer (PCET) steps at each pathway residue (**Figure 3**). The first step in RT is proposed to occur at the metal cofactor in β2, triggered by substrate and effector binding in α2 more than 35–40 Å away. Studies using site-specifically incorporated tyrosine analogs with altered reduction potentials; high-field, multifrequency electron paramagnetic resonance (EPR) methods; structural analysis; and RT photoinitiation in photosensitized RNRs (photo-RNRs) have provided insight into each of the proposed steps (7). Our current understanding of this pathway suggests that the thermodynamic landscape of the RT process (Y_{122}• to C_{439}) is uphill by greater than 200 mV and that the NDP reduction reaction, which also involves an uphill 3′-H atom abstraction, is driven to the right by rapid and irreversible loss of water during NDP reduction (**Figure 1*a***). This pathway design avoids buildup of highly reactive protein radical intermediates such as tyrosyl radical (Y•), which has a reduction potential of 0.96 V versus the normal H electrode. Reduction of any of the Y• intermediates in the pathway (**Figure 3**) would inactivate the RNR, leading to catastrophic consequences for the organism (23, 24). Accordingly, the RT pathway provides a target of opportunity for future drug design.

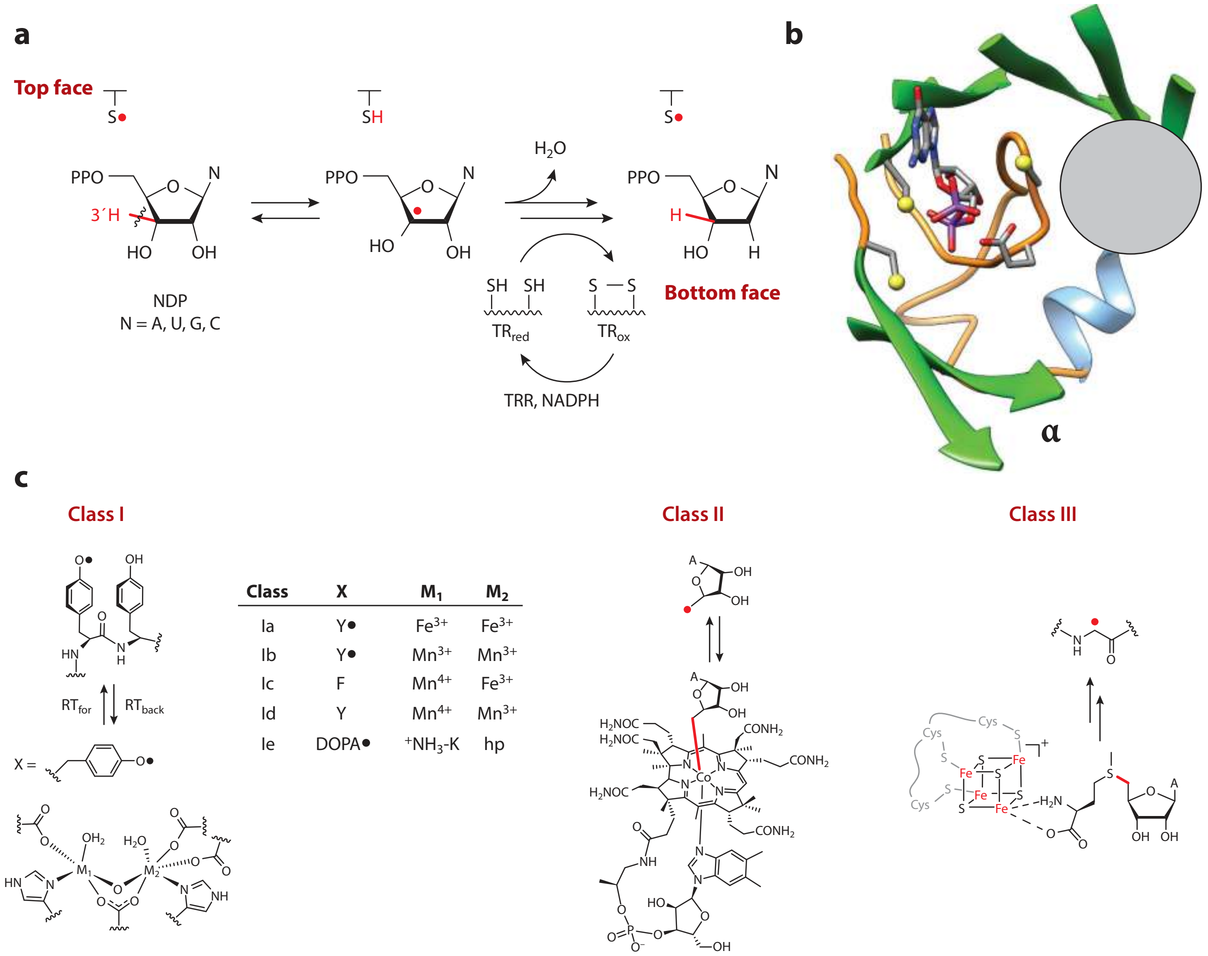

Class	X	M_1	M_2
Ia	Y•	Fe^{3+}	Fe^{3+}
Ib	Y•	Mn^{3+}	Mn^{3+}
Ic	F	Mn^{4+}	Fe^{3+}
Id	Y	Mn^{4+}	Mn^{3+}
Ie	DOPA•	$^{+}NH_3$-K	hp

Figure 1

(*a*) Ribonucleotide reductases (RNRs) catalyze the conversion of nucleoside 5′-diphosphates (NDPs) or triphosphates (NTPs) to deoxynucleotides (dNDP or dNTP). (*b*) The reduction occurs in the active site in subunit α, composed of a 10-stranded β-barrel with three cysteines and conserved placement of the oxidant (*gray circle*) involved in thiyl radical formation (–S•; top face in panel *a*) that initiates NDP reduction. The bottom-face thiols in panel *a* deliver the reducing equivalents and themselves become oxidized. (*c*) The oxidants are distinct among the RNR classes (I, II, and III), represented here by a gray circle juxtaposed with the –S• loop. The substrate and four essential residues, including the three essential cysteines and E_{441}, are shown as sticks. The class Ia RNRs use a diferric-tyrosyl radical (Y•) cofactor (M_1, M_2 = Fe^{3+}) that is located in subunit β (*left*, *bottom*) to generate a radical species in the active site in subunit α. The oxidation occurs over a distance of ∼35 Å by long-range radical transfer (RT) to first generate a Y• in subunit α (*under the gray circle* in panel *b*) and then generate –S• on an adjacent cysteine (top face in panel *a*). In other class I RNRs (Ib–Ie), oxidation also occurs by long-range RT across α and β but involves distinct metallo-oxidants (X, M_1, M_2). In class II and III RNRs, the oxidants, the 5′-deoxyadenosyl radical generated from adenosylcobalamin (class II), and the glycyl radical (class III) generated from *S*-adenosylmethionine and an FeS cluster are located adjacent to the cysteine to be oxidized (*gray circle* in panel *b*). Abbreviations: A, adenine base; TRR, thioredoxin reductase.

Evidence for the docking model (**Figure 2*c***) has been provided by trapping pathway radicals using tyrosine analogs with perturbed reduction potentials (**Figures 3** and **4*a***) and active-site radicals in α2 generated using mechanism-based inhibitors (MBIs) (**Figure 4*b***) (25). Pulsed electron–electron double-resonance (PELDOR) spectroscopy and negative-stain electron

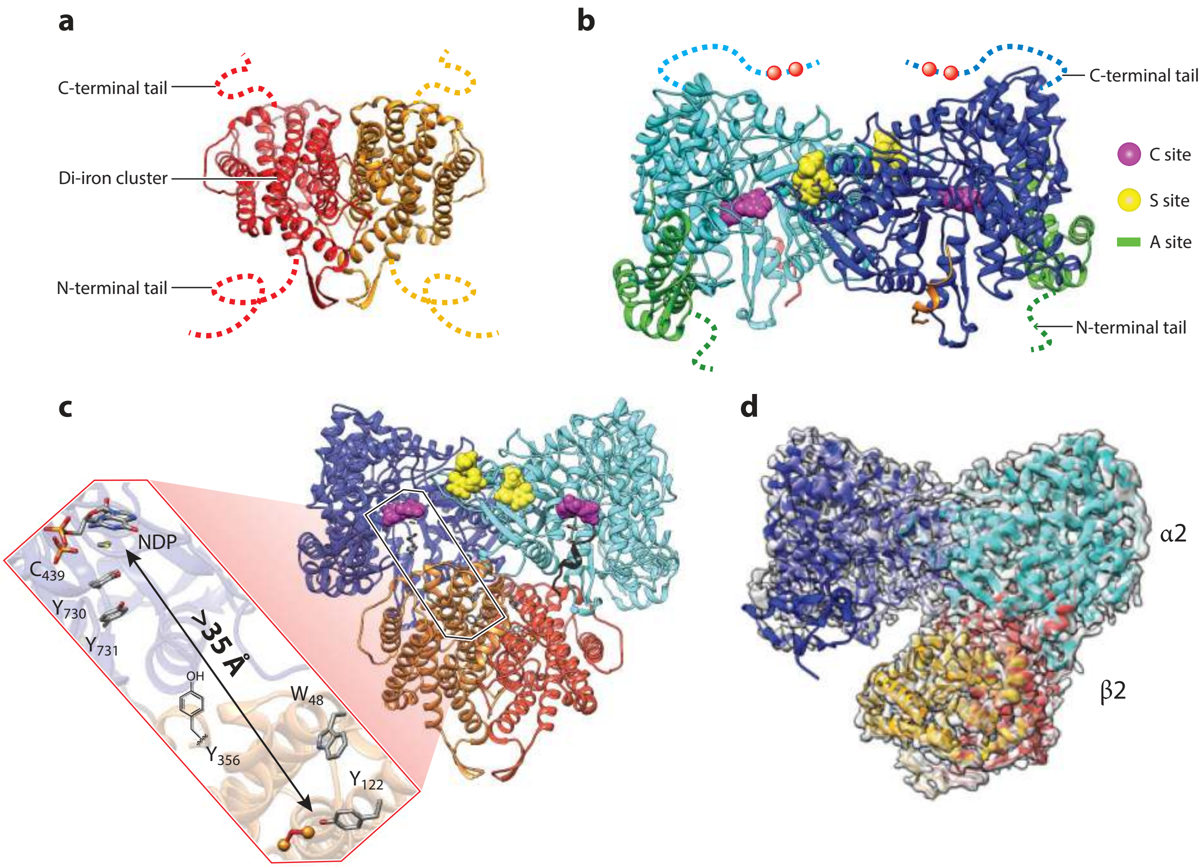

Figure 2

Structural models of the class Ia ribonucleotide reductase (RNR) from *Escherichia coli*. (*a*) X-ray structure of β2 (19), a homodimer (*red/orange*) with disordered C-terminal tail residues (341–375; *dashed lines*). (*b*) X-ray structure of α2 (13), a homodimer (*light/dark blue*) with disordered C-terminal tail residues (737–761; *dashed lines*) that houses the two cysteines (*red balls*) that rereduce the active-site disulfide formed on NDP reduction (see **Figure 1*a***). α2 also houses the A site (activity site or cone domain) that binds ATP (which activates the RNR) or dATP (which inactivates the RNR) (*green*); the C site (catalytic site) that binds cytosine, uridine, guanosine, and adenosine 5′-diphosphates (CDP, UDP, GDP, and ADP; collectively, NDPs) (*magenta*); and the S site (specificity site) that binds the effectors deoxyadenosine, adenosine, thymidine, and deoxyguanosine 5′-triphosphates (dATP, ATP, TTP, and dGTP) (*yellow*). (*c*) The Eklund docking model of α2β2 (13) with the long-range radical transfer pathway (*left*) (18). Also shown is a peptide (residues 360–375 of β2; *gray*) that is proposed to represent the tail of β2 responsible for α2 binding. (*d*) A cryo–electron microscopy (cryo-EM) structure of an active α2β2 complex with two mutations in β2: F_3Y_{122} and E52Q (11). The asymmetric complex forms when F_3Y_{122}/E52Q-β2 interacts with α2, GDP, and TTP. The 3.6-Å-resolution cryo-EM density structure is shown in transparent gray. This structure of the active α2β2 can be compared with the symmetric docking model in panel *c*.

microscopy (EM) (**Figure 2*c***) have enabled spectroscopic and structural analysis, respectively, of these trapped α2β2 complexes (see the next section).

3-Aminotyrosine–RNR and Pulsed Electron–Electron Double-Resonance Analysis: Low-Resolution Evidence for the Docking Model

3-Aminotyrosine (NH_2Y) is easier to oxidize than Y by 590 mV (**Figure 4*a***). When NH_2Y replaces a pathway Y in α or β and is incubated with the second subunit, substrate, and specificity effector,

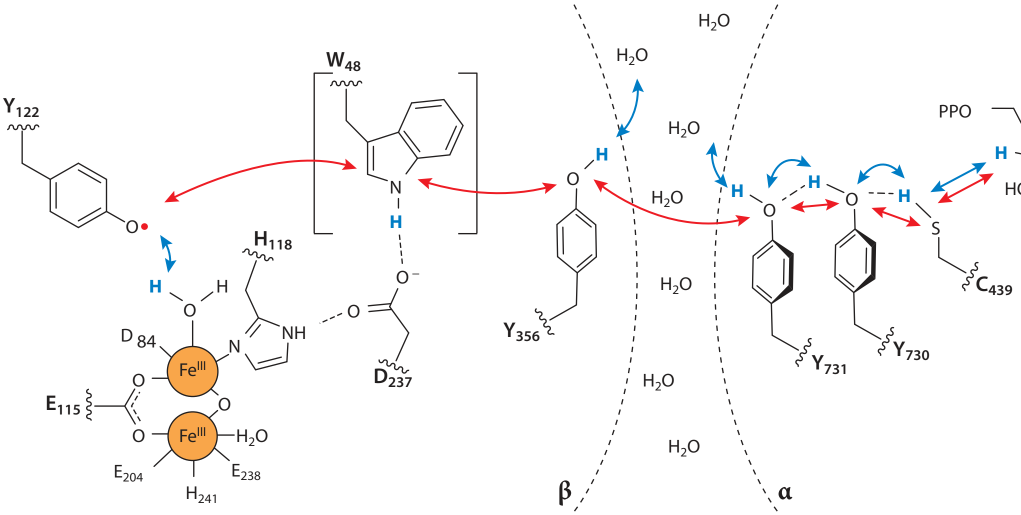

Figure 3

Proposed radical transfer (RT) pathway in class Ia ribonucleotide reductases (RNRs) (*Escherichia coli* numbering) within the α2β2 complex. Binding of substrate and allosteric effector (not shown) to α2 triggers RT from the Y_{122}• of the $Fe^{3+}{}_2$-Y_{122}• cofactor in β through three transient Y•s (356-β across the subunit interface to 731-α and 730-α). The Y_{730}•-α (see **Figure 1*b***) then oxidizes the active-site cysteine to a –S• that initiates NDP reduction (see **Figure 1*a***). Subsequent to dNDP formation, the Y_{122}• is regenerated by reverse RT. W_{48}-β appears in brackets because its role in the pathway has not been established. Each step in the pathway is proposed to involve distinct proton (H^+, *blue arrows*)-coupled electron (e^-, *red arrows*) transfer steps (7).

Mechanism-based inhibitor (MBI): nucleotide that binds to the active site of an RNR, leading to its 3′ C–H bond cleavage by hydrogen atom abstraction and subsequently to distinct radical chemistry and enzyme inactivation

Pulsed electron–electron double resonance (PELDOR) spectroscopy: a paramagnetic resonance method that allows measurement of distances (15 to 100 Å) between two paramagnetic species that experience weak dipolar interactions

it functions as an efficient radical trap, forming a 3-aminotyrosyl radical (NH_2Y•) (10, 25) that is unable to oxidize the next residue in the pathway. Under these conditions, 0.5 equivalents of total Y_{122}• in β2 are reduced, and a stoichiometric amount of NH_2Y• is formed in one α/β pair of the α2β2 complex (**Figure 5*a***). Since further chemistry in this α/β pair is prevented, as is the conformational switching to allow initiation of chemistry on the adjacent α/β pair, 0.5 equivalents of Y_{122}• still reside in the adjacent α/β pair. These results require asymmetry within α2β2 and are the basis for our definition of half-site reactivity.

In these trapped complexes, PELDOR spectroscopy has been used to measure the distance between the NH_2Y• (located at 356-β or at 731-α or 730-α) in one α/β pair and the Y_{122}• in the adjacent pair (**Figure 5*a***). Studies with the MBI 2′-azido-2′deoxycytidine diphosphate (N_3CDP) (**Figure 4*b***), which forms a nitrogen-centered radical (N•) covalently bound to a cysteine in the active site of α2, also allow a distance measurement (**Figure 11**). Additionally, RNR mutants in which Y_{122}• is replaced with 2,3,5-F_3-Y_{122}• or NO_2Y_{122}• (**Figure 4*a***), which are "hotter" oxidants than Y_{122}•, also generate pathway radicals and demonstrate half-site reactivity (26). **Table 1** summarizes the distances measured to date; they are consistent with the docking model (**Figure 2*c***) (25, 26). An unexpected outcome of these experiments was that when radicals were trapped within the pathway, the α2β2 complex exhibited increased subunit affinity, thus enabling its isolation. A number of these complexes have been examined by negative-stain EM and have revealed structures resembling the docking complex (15–30-Å resolution) (**Figure 5*b***) (7). Our current model from these studies with perturbants is that for wild-type RNR, both RT and catalysis occur initially within one α/β pair of an asymmetric α2β2, which triggers rapid chemistry within the second α/β pair. The mechanism of switching remains to be determined.

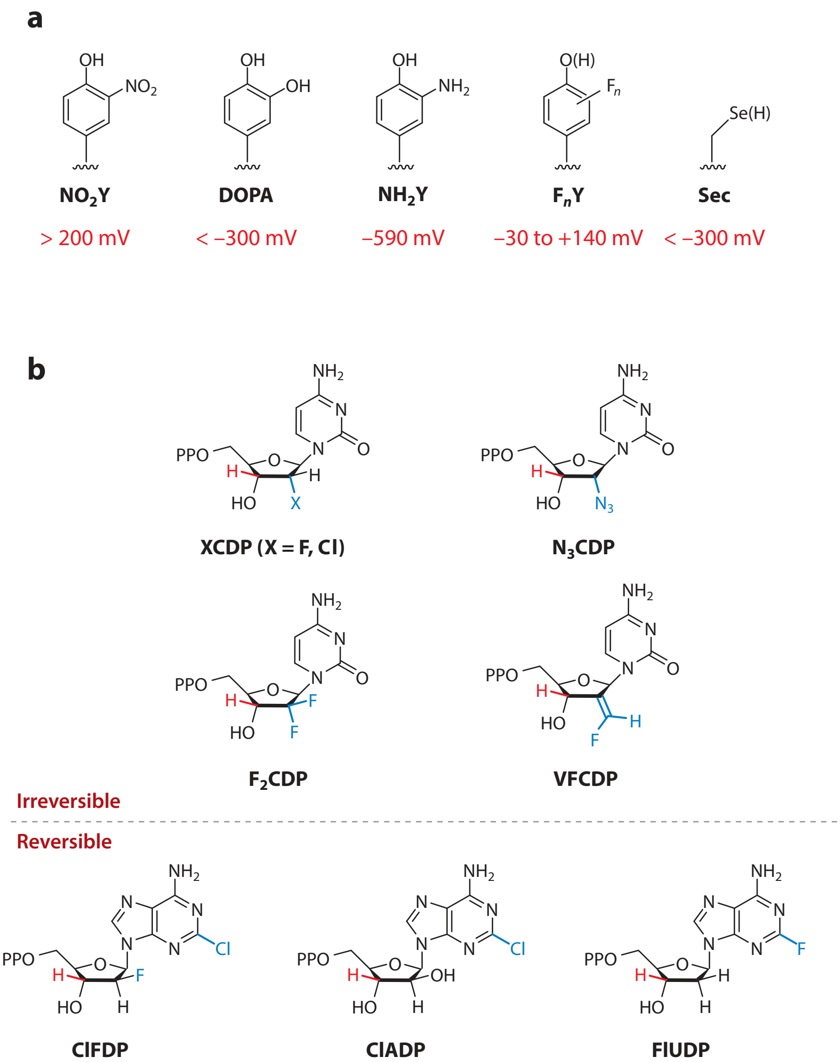

Figure 4

Structures of unnatural amino acids and nucleotide analogs used to study class Ia ribonucleotide reductases (RNRs). (*a*) Unnatural amino acids that have been site-specifically incorporated in place of the tyrosines (Ys) or cysteine within the radical transfer pathway (see **Figure 3**) as well as their reduction potentials versus Y for NO_2Y, 2,3-dihydroxy-phenylalanine (DOPA), 3-aminotyrosine (NH_2Y), and fluoride-substituted tyrosines (F_nYs) (24) and versus cysteine for seleocysteine (Sec) at pH 7. NH_2Y is 590 mV easier to oxidize than Y. Fluorinated Ys (F_nYs, where $n = 2$ or 3) enable tuning of the reduction potential over 170 mV depending on the number of Fs and their substitution pattern. (*b*) Nucleoside 5′-diphosphates can be irreversible and reversible inhibitors of RNR. The irreversible inhibitors are mechanism-based, as the 3′ C–H bond (*red*) of the inhibitor must be cleaved, as with the normal substrate (see **Figure 1*a***), before distinct radical chemistry in each case occurs, causing enzyme inactivation. The nucleosides (FC, N_3C, F_2C, VFC, ClF, ClA, FlU) are utilized therapeutically and are metabolized to the diphosphates (PPO). The inhibitors of RNR are shown.

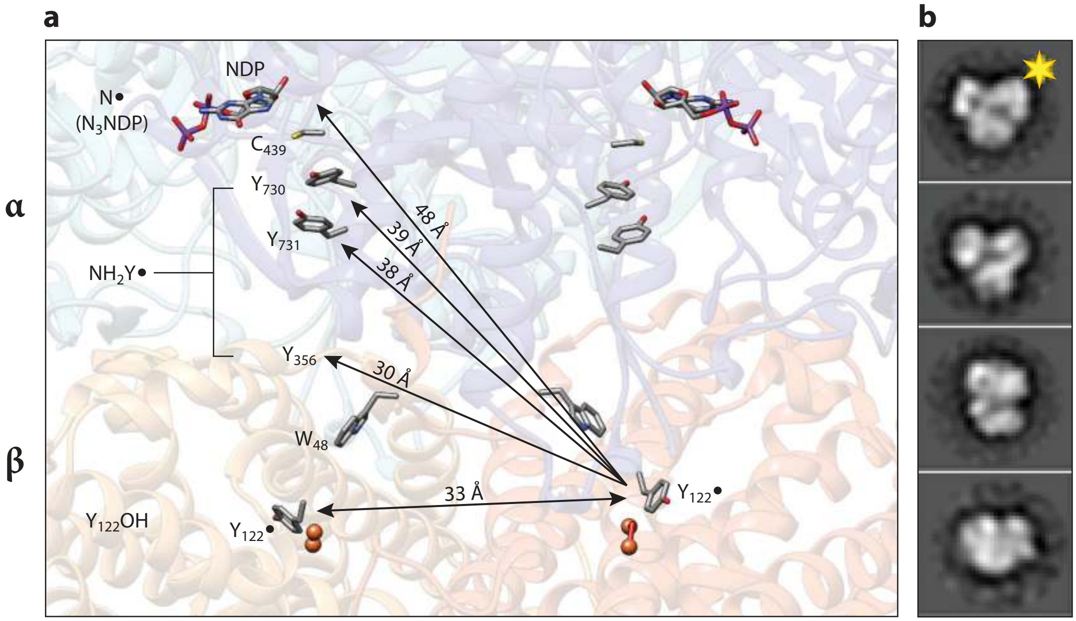

Figure 5

Support for the Eklund docking model (see **Figure 2*c***). (*a*) Pulsed electron–electron double-resonance spectroscopy used to measure distances between Y_{122}• in the unreacted α/β pair (*right*) and the trapped radicals (NH_2Y• or N•) in the reactive α/β pair where Y_{122} is reduced (YOH) (*left*). (*b*) Representative negative-stain electron microscopy 2D class averages of the structures of the NH_2Y_{730}• trapped in an α2β2 complex (25). The view with the yellow star resembles the Eklund docking model shown in **Figure 2*c***.

HIGHER-RESOLUTION STRUCTURES OF RNRs

Inhibited Structures In Vitro

dATP is a universal inhibitor of all class Ia RNRs. It binds to the N-terminal domain of α (**Figure 2*b***). Two independent studies by the Dealwis and Walz groups (8) and the Drennan and Asturias groups (27) in 2011 and 2018, respectively, revealed structures of eukaryotic dATP-inhibited states. In a study of *Saccharomyces cerevisiae* RNR, Fairman et al. (8) observed an α6 hexameric ring structure crystallographically (6.6 Å). In a study of human α with CDP, dATP, and a small amount of ATP, Brignole et al. (27) observed by cryo–electron microscopy (cryo-EM) a similar but higher-resolution hexameric ring structure (3.3 Å) (**Figure 6*b***). Both groups also reported negative-stain EM studies (28 and 30 Å) of a dATP-inhibited state in the presence of both α and β (1:1). Despite the stoichiometry of the subunits, in both cases less than one β2/α6 was observed. Both eukaryotic dATP-inhibited states are a trimer of dimers, with the cone domains responsible for the dimer interfaces. In addition, in human RNRs, small-angle X-ray scattering data on this state suggested that β2 could not enter the hole in the α6 ring structure, implying that an active α2β2 is not accessible (28).

EM: electron microscopy

NH_2Y: 3-aminotyrosine

NH_2Y•: one-electron-oxidized 3-aminotyrosine

The structure of the dATP-inhibited *E. coli* Ia RNR generated from α:β (1:1) in the presence of dATP is distinct from its eukaryotic counterparts. Using a variety of biophysical methods, Drennan and colleagues (29, 30) reported an α4β4 ring complex with alternating α2s and β2s and a hole in the center (**Figure 6*a***). In this structure, in contrast with the eukaryotic inhibited state, the cone domain interacts with β2. The most intriguing result is that the distance between Y_{122}•-β2 and C_{439} in α2 (**Figure 2*c***) has increased from 35 to 60 Å, shutting down RT and, consequently,

Table 1 Pathway radicals trapped in the *Escherichia coli* class Ia ribonucleotide reductase by site-specifically incorporating unnatural amino acids or reaction with N_3UDP; pulsed electron–electron double-resonance distances (< ±1 Å) are given in the last column. The red dot corresponds to forward radical transfer (RT) and the blue dot to reverse RT, as indicated by the direction of the arrows on the pathway shown below the table

α	β	Y_{122}	Y_{356}	Y_{731}	Y_{730}	C_{439}	NDP	Y_{122}•–X• distance (Å)
WT	WT	🔴/🔵	—	—	—	—	—	33
WT	$DOPA_{356}$	—	🔴	—	—	—	—	30
WT	NH_2Y_{356}	—	🔴	—	—	—	—	30
$Y_{731}F$	F_3Y_{122}	—	🔴	—	—	—	—	30
NH_2Y_{731}	WT	—	—	🔴	—	—	—	38
$NH_2Y_{731}/R_{411}A$	WT	—	—	🔴	—	—	—	35
NH_2Y_{730}	WT	—	—	—	🔴	—	—	39
WT	WT	—	—	—	—	—	N_3UDP🔴	48
WT	F_3Y_{122}	—	🔵	—	—	—	—	30
WT	NO_2Y_{122}	—	🔵	—	—	—	—	30

Abbreviations: NDP, nucleoside diphosphate; WT, wild-type.

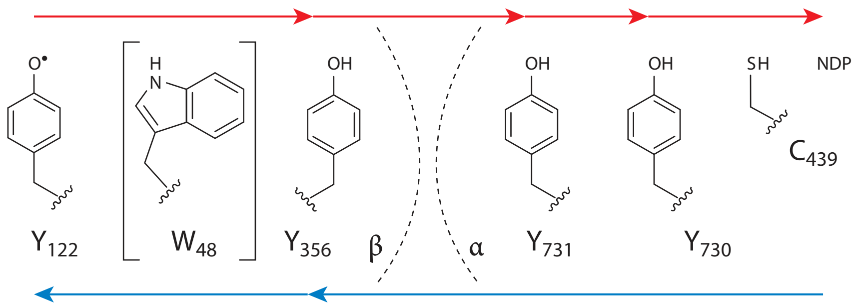

nucleotide reduction. Thus, despite the distinct quaternary structures of the dATP-inhibited states, a common mechanism of inhibition emerges that involves inability of β2 to form an active α2β2 state.

Inhibited Structures In Vivo

The presence of these inhibited states in cells (**Figure 6**) is important to establish. Drennan and colleagues (31) used their structural insight from the *E. coli* α4β4 complex and site-directed mutagenesis to disrupt the α2/cone domain/β2 interface. Activity assays and negative-stain EM analysis of several mutants showed that dATP no longer inhibited RNR, and no α4β4 was detected. This study, in concert with genetic experiments on *E. coli* using a random mutagenesis protocol, a screen

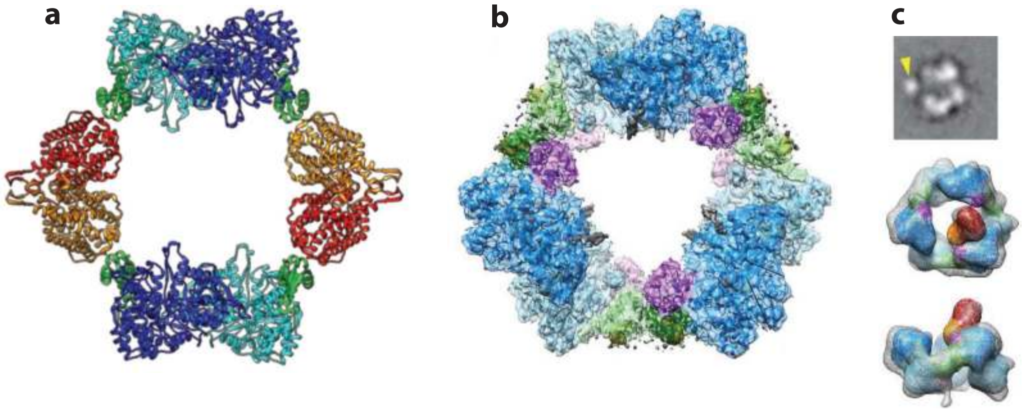

Figure 6

Structures of dATP-inhibited states of class Ia ribonucleotide reductases (RNRs). (*a*) The X-ray structure of a dATP-inhibited *Escherichia coli* class Ia RNR (29) is an α4β4 ring structure with a hole in the middle, composed of alternating α2 (*light/dark blue*, with the cone domains in *green*) and β2 (*orange/red*) subunits. Note the importance of the cone domain in the α/β interaction. (*b*) The cryo–electron microscopy (cryo-EM) structure of a dATP-inhibited human class Ia RNR (27) is a hexameric α6 ring with a hole in the middle. The α subunits are in light and dark blue, the cone domain is in light and dark green, and a three-helix insertion is in purple (residues 638–681). Note the importance of the cone domain in the α/α interactions. (*c*) Cryo-EM structure of an α/β (1:1) clofarabine triphosphate (ClFTP)-inhibited human class Ia RNR (27). (*Top*) Representative cryo-EM 2D class-average images generated from α, β, and ClFTP that show β (*arrow*) interacting with α. (*Middle*, *bottom*) Two views of the 3D reconstruction of the same data set. The bottom image is rotated 90° from the middle image. Only a fraction of the α6 rings in these images have a single and variably positioned β.

for altered dNTP pools, and genome sequencing, identified RNR with mutations at the same interface (32). Together, these biochemical and genetic studies suggest that the dATP-inhibited state of *E. coli* α4β4 occurs in vivo. Studies with clofarabine (ClF) (33) and other nucleoside therapeutic inhibitors of RNR [cladribine (ClA) and fludarabine (FlU)] (34) (**Figure 4*b***) have demonstrated α6 formation in several human cell lines treated with sublethal doses of the nucleosides (35). The distinct inhibitory structures of the Ia RNRs (**Figure 6**) are discussed further in the section titled Use of Mechanism-Based Inhibitors and Reversible Inhibitors to Understand the Mechanism and Design of New Therapeutics, below.

Toward Active α2β2 Structures

Our studies using fluorinated (F) tyrosine analogs (**Figure 4*a***), combined with bioinformatics and the docking model of α2β2 (**Figure 2*c***) to identify residues within the α/β subunit interface including E52 in β, led us to investigate the *E. coli* double mutant of β2 (E52Q and F_3Y_{122}•) (11). The F_3Y_{122} substitution allowed trapping of the Y_{356}• on the RT pathway (**Figure 3**) that resulted in a tighter subunit affinity, that is, the K_d < 0.4 nM as compared with 0.2 μM for the control with E52Q-β2 (36). Although incubation of E52Q-β2 with any substrate and effector resulted in a completely inactive RNR, incubation of the double mutant of β2 (E52Q and F_3Y_{122}•) with α2 (or His_6-α2), GDP, and TTP unexpectedly produced 0.5 equivalents of Y_{356}• and 0.5 equivalents of dGDP, consistent with half-site reactivity (36). The resulting α2 (E52Q and F_3Y_{122}•β2) complex gave rise to a near-atomic-resolution (3.6-Å) cryo-EM structure (**Figure 2*d***) that is asymmetric, consistent with half-site reactivity. In line with the biochemistry, the structure of α shown in the left side of **Figure 2*d*** has generated a disulfide in the active site that we presume gave rise to dGDP. With the α/β pair shown on the right side of **Figure 2*d***, residues 341–375 in β have been visualized for the first time (**Figure 2*a***). In addition, GDP and TTP are apparent, and the location of the

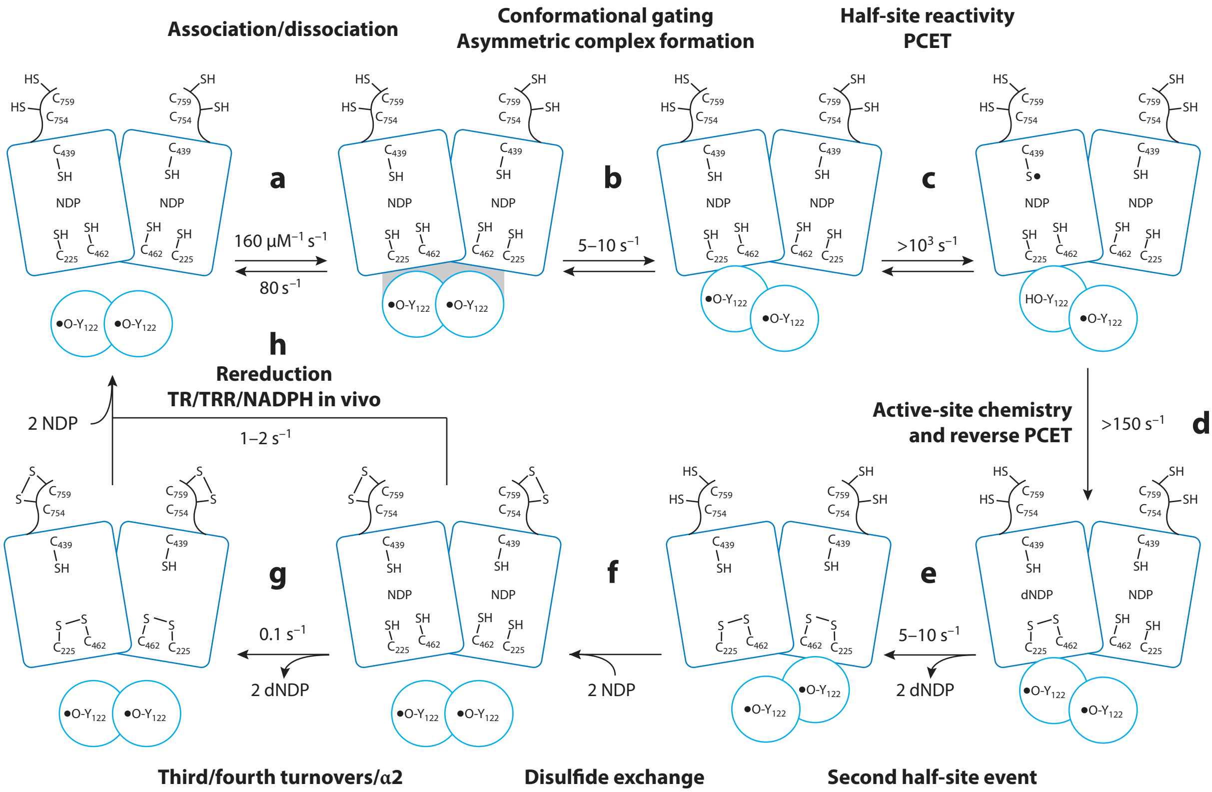

Figure 7

Resetting ribonucleotide reductases for single and multiple turnovers for 2′-deoxynucleoside diphosphate (dNDP) formation. The model assumes an α:β ratio of 1:1, that Y_{122}• is distributed equally between each β of β2, and that the wild-type α2β2 complex is asymmetric. In the absence of external reductants, two dNDPs generated at a rate of 2 s^{-1} (substrate only) to 5–10 s^{-1} (substrate and effector) arise from chemistry at each α of α2 (*e*). Steps *b* and *e* are rate limiting and conformationally gated. In an assay in the absence of an external reductant, two additional dNDPs are formed at 0.1 s^{-1} (*g*). In the presence of an external reductant such as thioredoxin (TR) and thioredoxin reductase (TRR), under steady-state conditions, step *h* becomes rate limiting. Other steps include (*a*) binding of substrate- and effector-bound α2 with β2; (*c*) rapid radical transfer to generate the C_{439}–S•; (*d*) active site chemistry, dNDP formation, and reverse radical transfer; and (*f*) reversible reduction of the active site disulfide by the cysteines in the C-terminal tail of α and binding of two additional NDPs.

pathway residue Y_{356} is revealed for the first time as part of the entire RT pathway (11) (**Figures 2*c*** and **3**). Our ability to trap radicals at different residues within the pathway summarized in **Table 1** and the increased subunit affinity observed under these conditions suggest that this approach may lead to additional cryo-EM structures that will provide insight into the dynamics of this amazing machine and the switching mechanism between the two α/β pairs.

NEW MECHANISTIC INSIGHT INTO THE CHEMISTRY OF NDP REDUCTION

Model for Disulfide Rereduction and Conformational Gating

In the *E. coli* RNR, the rate-limiting step (or steps) for dNDP formation (**Figure 7*b*,*e***) is physical, involving conformational changes that mask the chemistry of long-range reversible RT and dNDP

ISSUES AFFECTING SCREENS TO DISCOVER RNR INHIBITORS

The model for RNR-mediated NDP reduction shown in **Figure 7** encompasses weak and dynamic subunit interactions that change with subunit and dNTP concentrations. These changes alter RNR's quaternary structure(s) and activity. These issues are essential to understand to successfully develop *E. coli* RNR (42) assays in vitro and in vivo for high-throughput screens for RNR inhibitors. The same issues are likely to be encountered with other class Ia and Ib RNRs.

formation (22, 37). The observed rate constants (k_{cat}) for dNDP formation in the absence of an external reductant (**Figure 7*a–e***) range from 2 to 5–10 s^{-1} with substrate and substrate/effector, respectively. In the presence of the physiological reductants (in cells or in steady-state assays), additional conformational changes become rate limiting (1–2 s^{-1}; **Figure 7*b***) and likely involve α/β subunit dissociation, conformational changes associated with the rereduction of the active-site disulfide by the C-terminal tail of α (**Figure 7*f–h***), or both, and are protein concentration dependent. Different αs have distinct cysteine configurations within their C-terminal tails (**Figure 2*b***) and require organism-specific reductants [e.g., thioredoxin (TR), NrdH, glutaredoxin, thioredoxin reductase (TRR), and glutaredoxin reductase] (38–41).

Multiple methods have been employed to unmask the mechanistic details of dNDP formation. These include site-directed mutagenesis, insertion of unnatural amino acids (**Figure 4*a***), photo-RNRs (photo-β2), and MBIs (**Figure 4*b***). In subsequent sections, we describe how this information, combined with structural studies, has provided insight into new therapeutic strategies (see the sidebar titled Issues Affecting Screens to Discover RNR Inhibitors).

TR: thioredoxin

TRR: thioredoxin reductase

Unnatural amino acids: tyrosines with altered reduction potentials and pK_as used as tools to study PCET

NDP Reduction Mechanism

Figure 8 depicts our current proposed mechanism for nucleotide reduction (5, 43). Steps designated *a–e* describe the main chemical transformation, whereas the numbers show the proposed chemistry that occurs to the NDP and the active site protein residues, **1–6**. The important features are that an –S• (C_{439}, *E. coli*) initiates reduction of NDP by removal of its 3′-H to form a 3′-nucleotide radical (**2**) (**Figure 8*a***) (44). E_{441} facilitates this step by functioning as a general base catalyst for 3′-OH deprotonation (45). This reaction is driven to the right by the rapid, irreversible loss of water (**2** to **3**) catalyzed by C_{225} (**Figure 8*b***). The proposal for the reductive half-reaction (**Figure 8*c,d***) is that the 3′-keto-2′-radical generated subsequent to water loss is reduced by PCET to generate the 3′-ketodeoxynucleotide and the three-electron, disulfide radical anion (**Figure 8*c***, conversion of **3** to **4**). The disulfide radical anion then reduces 3′-ketone by another PCET step (**Figure 8*d***), in which the proton is supplied by the protonated E_{441}. Finally, the H atom abstracted from the 3′ position of NDP in the first step is returned to the same position (step *e*) to form dNDP and the C_{439}• that reoxidizes Y_{122} in β2 on each turnover.

Role of multiple thiyl radicals. The role of the –S• initiator (C_{439}) (**Figure 8**) was previously established on the basis of studies of the class II adenosylcobalamin-dependent ribonucleotide triphosphate reductase. An exchange-coupled –S•-cob(II)alamin species, detected by EPR and UV-visible absorption stopped-flow spectroscopies, was shown to be chemically and kinetically competent in deoxynucleotide formation (46, 47). The structural homology and conserved residues in the active site of all RNRs (**Figure 1*b***) have thus been used to infer the universal involvement of –S• in initiating 3′-H atom abstraction (14). Support for the involvement of –S• in the reductive half-reaction (**Figure 8*c,d***) comes from studies with E441Q-α/β/CDP/TTP in

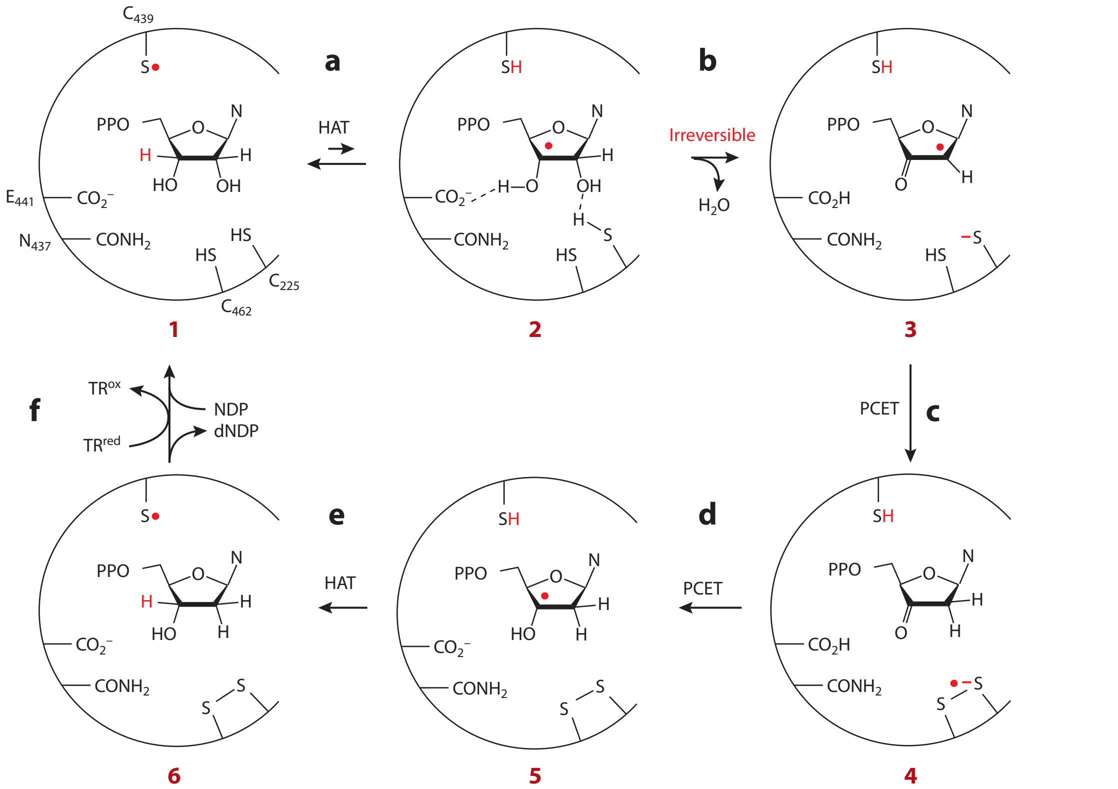

Figure 8

Mechanism of –S• mediated NDP reduction by most ribonucleotide reductases (5). *a–f* indicate the proposed steps in the reaction, and numbers **1–6** indicate the active-site participants in each step. (*a*) An –S• (C_{439}, *Escherichia coli*) initiates reduction by removal of the NDP 3′-H. (**1**,**2**) E_{441} facilitates this step by functioning as a base catalyst for 3′-OH deprotonation. (*b*) This reaction is driven to the right by the rapid, irreversible loss of water catalyzed by C_{225}. (*c*,*d*) The 3′-keto-2′-radical (**3**) is reduced by proton-coupled electron transfer (PCET) to generate the 3′-ketodeoxynucleotide and the three-electron, disulfide radical anion (**4**). (*d*) This species then reduces 3′-ketone by another PCET step. (*e*) The H atom abstracted from the 3′ position of NDP is returned to the same position to form dNDP and the C_{439}• that reoxidizes Y_{122} in β2 on each turnover. (*f*) The rereduction of the active site disulfide is proposed to occur, as described in **Figure 7**. Note that steps *a*, *c*, *d*, and *e* involve either H atom transfer (HAT) or PCET processes. Other abbreviation: TR, thioredoxin.

which a disulfide radical anion was spectroscopically identified due to the absence of a required proton from E_{441} for the PCET (**Figure 8*d***) (48). Although –S• chemistry has been proposed for many enzymatic reactions, RNR is the only enzymatic system in which this intermediate has been detected (46, 47).

Photo-RNRs unmask rate constants for NDP reduction chemistry. The development of methods to uncouple conformational gating (49, 50) and unmask chemistry (23, 26) has allowed unprecedented insight into active-site chemistry, including –S• mediated H atom abstraction (**Figure 8*a***) and the subsequent rate-limiting 3′-ketodeoxynucleotide reduction (**Figure 8*d***, **4** to **5**). In the former case, we designed a method for photosensitization of RNRs (**Figure 9*a***) in which a photooxidant, bromomethylpyridyl rhenium(I) tricarbonyl phenanthroline ([Re]), is covalently attached to a single surface-exposed cysteine in the S355C-β2 mutant; the Y_{122}• in β2 is reduced and Y_{356} in β2 is replaced with a fluorinated tyrosine (F_nY_{356}) (**Figure 4*a***). This photo-β2, in

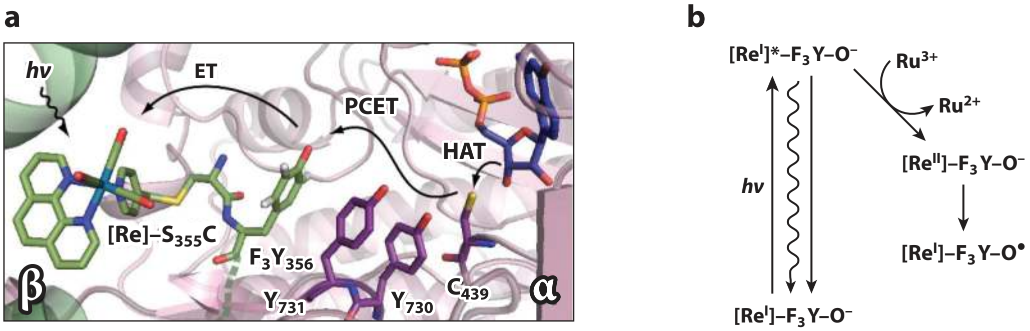

Figure 9

Use of photosensitized ribonucleotide reductases to unmask rates of chemical steps. (*a*) Schematic of photo-β2 with rhenium photooxidant [Re] attached covalently to C_{355} and Y_{122}OH-β2 (i.e., Y_{122}• is reduced) in complex with cytidine diphosphate (CDP), adenosine triphosphate (ATP), and α2 (49). In the case shown, the Y_{356} in β is replaced with the unnatural amino acid 2,3,5-F_3Y_{356} (see **Figure 4**). (*b*) Light initiates the reaction, and the presence of the flash quencher, $Ru(NH_3)_6Cl_3$, prevents charge recombination (*left*) and generates $[Re^{II}]$–F_3Y–O^- (*right*), which rapidly drives 2,3,5-F_3Y_{356} oxidation to the 2,3,5-F_3Y_{356}• that initiates chemistry within α2. The different mechanisms of oxidation shown are electron transfer (ET), proton-coupled electron transfer (PCET), and H atom transfer (HAT).

complex with α2, substrate, and effector, can be rapidly (within nanoseconds) oxidized to an F_nY_{356}•-β2 state upon illumination (**Figure 9*b***). The photochemically generated radical rapidly equilibrates with the RT pathway in α2, ultimately oxidizing C_{439} and initiating cleavage of the 3′ C–H bond of NDP. Comparison of the F_nY_{356}• decay, observed by transient absorption spectroscopy in the presence of 3′-[^{1}H]-CDP or independently in the presence of 3′-[^{2}H]-CDP, established a lower limit for the –S• mediated H atom abstraction (**Figure 8*a***) of 1.3×10^4 s^{-1} and an isotope effect of ≥7 (51). Note that the k_{cat} for RNR is 2–10 s^{-1}. The RT chemistry is thus very fast and was revealed for the first time using this method.

The subsequent rate-limiting 3′-ketodeoxynucleotide reduction (**Figure 8*d***) has been examined by incorporating tyrosine analogs with altered reduction potentials in place of Y_{122} in β. Use of these "hotter" oxidants drives RT and also uncouples conformational gating. Specifically, F_3Y_{122}• and NO_2Y_{122}• (**Figure 4*a***) have higher reduction potentials than the native Y_{122}•(β2) by 80 and >200 mV, respectively (23, 26), as determined from independent measurements of formal reduction potentials in a small three-helix-bundle protein (24). These β2 mutants have been studied in an effort to observe the slow step(s) within the proposed chemistry, specifically PCET reduction of the 3′-ketone by the disulfide radical anion (**Figure 8*d***). When NO_2Y_{122}•-β2 (or F_3Y_{122}•-β2) is mixed with α2/CDP/ATP, dCDP formation occurred at ∼150 s^{-1} (or 30 s^{-1}). This rate constant is similar to the 50 s^{-1} measured for dCTP formation; the latter is catalyzed by class II RNRs (52), where the active-site chemistry is not masked by physical steps and is much faster than the wild-type turnover number of 1–2 s^{-1}.

USE OF MECHANISM-BASED INHIBITORS AND REVERSIBLE INHIBITORS TO UNDERSTAND THE MECHANISM AND DESIGN OF NEW THERAPEUTICS

The MBIs 2′-halo-(X)-2′-deoxyNDPs (XNDP, where X = Cl or F) (**Figures 4*b*** and **10**) have played a pivotal role in our current understanding of the mechanism of nucleotide reduction (53). In 1976, Thelander et al. (54) reported that 2′-chloro-2′-deoxycytidine diphosphate (ClCDP) incubated with the *E. coli* RNR resulted in time-dependent release of Cl^- and cytosine and that the

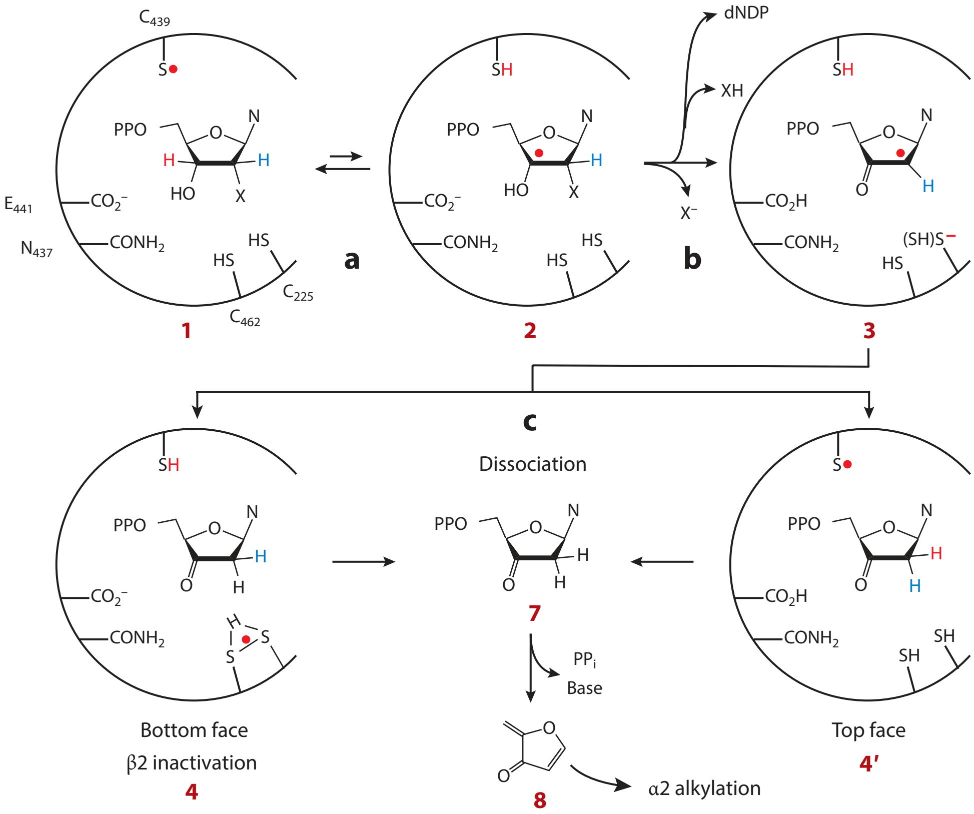

Figure 10

Generic mechanism for 2′ X-dNDP (where X = F, Cl, N_3, or F_2) (see **Figure 4**) mechanism-based inhibition of ribonucleotide reductases with loss of X^- in step *b* (43, 53). **3** is formed with the bottom-face protonation states of the thiols unknown. The intermediate 2′-nucleotide radical can be reduced from the top face by SH of residue 439 to produce **7** (*right*) or the bottom face to produce **7** (*left*) through intermediates **4** and **4′**; both of these dissociate from the active site and decompose to generate the products (PP_i, base, and **8**). **8** can alkylate the α subunit. Alternatively, if in conversion of **2** to **3** (step *b*) XH is eliminated, then the same product produced by the reduction of NDP, that is, deoxynucleotide (dNDP), is formed. *a–c* describe the steps proposed for the conversion of the inhibitor to intermediate **7**. The numbers **1–4** and **4′** represent the proposed structures of the nucleotide intermediates and the protein environment. Other abbreviation: XH, protonated form of the leaving group.

α subunit was inactivated. These observations provided the impetus for studies using isotopically labeled nucleotide analogs, which led to the general model for inhibition shown in **Figure 10**. As with the NDP substrate, the –S• abstracts the 3′-H (**Figure 10*a***) to generate **2**. The outcome of the reaction depends on whether and how the loss of X at 2′-C is catalyzed by the enzyme. From **3**, the 2′-delocalized radical can be reduced from the top face (**4′**) by H atom transfer mediated by C_{439} or the bottom face (**4**) facilitated by C_{225}. With Cl(F)NDP, a 3′-ketodeoxynucleotide is generated (**7**) that dissociates from the active site (when X is not protonated). Intermediate **7** can decompose on a minute timescale to a nucleic acid base, pyrophosphate (PP_i), and a furanone (**8**) that nonspecifically alkylates the α subunit. If the reduction of the nucleotide intermediate in **3** occurs from the top face by C_{439} (**4′**), then reverse RT can effectively regenerate the Y_{122}• in β2. However, if reduction of this same intermediate occurs from the bottom face (**4**), Y_{122} remains reduced and β2 is inactivated. Thus, α and/or β can be inactivated via distinct mechanisms. With both XNDPs, if X is protonated (**Figure 10*b***), then dNDP is formed. The details of RNR inactivation in vitro and in vivo depend on the identities of the substrate and effector, leaving group (X), and reductant. In all cases, α inactivation requires Y_{122}• reduction. These inhibitors inactivate class I, II, and III RNRs by a common mechanism, suggesting similar active sites (**Figure 1*b***). The involvement of the α C-terminal cysteines in enzyme inhibition (**Figure 2*b***) is not well understood, as their covalent linkage to **8** is reversible, precluding isolation and characterization of alkylated α.

In contrast to XNDPs (X = Cl or F), a number of MBIs (X = N_3, F_2, or VF) (55–57) (**Figure 4*b***) share similar chemistry in steps *a* and *b* (**Figure 10**), but then undergo distinct chemistry controlled by X and the residues and their protonation states in the active-site cavity. Unraveling the mechanism by which N_3NDP inactivates all RNRs has defined the strategy to study the mechanism of action of the clinically used nucleoside therapeutics gemcitabine (F_2C) and ClF. F_2CDP is an irreversible inhibitor (58), and ClFDP and ClFTP are reversible, noncovalent inhibitors of RNRs (59–61) (**Figure 4*b***).

2′-Azido-2′-Deoxynucleotide

N_3NDPs (N = C, U, or A) are MBIs first reported by Thelander et al. (54). Extensive studies with N_3UDP (**Figure 11*a*,*b***) revealed that its incubation with α2β2 resulted in rapid loss of ∼90% RNR activity concomitant with the loss of only 0.5 equivalents of Y_{122}•. The total Y• loss was biphasic; the fast phase was accompanied by formation of N_2 gas and a nucleotide-based N•, derived from the N_3 moiety of N_3UDP. The N• was structurally characterized using isotopically labeled N_3UDPs and EPR methods. The nucleotide N• species then slowly decomposes to form a nucleoside base (blue N in **Figure 11*a***), PP_i, and **8** (62, 63). The α/β subunits then dissociate, and subsequent to α2β2 complex reformation, additional Y• is lost and more N• is formed. The recent examples of half-site reactivity (**Table 1**) and RNR asymmetry (**Figure 2*d***) suggest an explanation for the observation that 1 equivalent of inhibitor per α2β2 results in >90% loss of enzyme activity (53).

In vitro, N_3CDP inhibits β2 by reduction of the essential Y_{122}•, whereas in vivo, the nucleoside analog 2′-azido-2′-deoxycytidine (N_3C) is not cytotoxic. In cells, N_3C is not readily

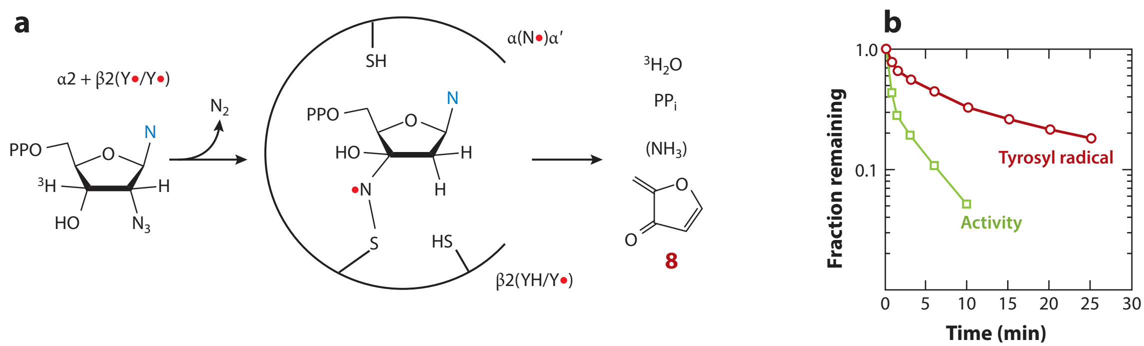

Figure 11

2′-Azido-2′-deoxynucleoside diphosphate (N_3NDP) (**Figure 4*b***) is a potent inhibitor of all class Ia ribonucleotide reductases (RNRs) (62, 63). Studies of this inhibitor provided a glimpse of unprecedented chemistry associated with reactive radical species in an active-site cavity and the challenges associated with radical structure elucidation. These studies also provided early evidence for half-site reactivity. The products formed during the inactivation include: N_2, NH_3, PP_i, and the furanone **8**, all initiated by 3′-C–H bond cleavage, resulting in ^3H_2O. (*b*) The kinetics of loss of RNR activity and tyrosyl radical during the inactivation are biphasic.

phosphorylated to N_3CMP by deoxycytidine kinase, demonstrating the importance of the specificity of this and other kinases in generating nucleotide (di- and triphosphate) therapeutics.

SEC: size-exclusion chromatography

Gemcitabine and Clofarabine: Clinically Used Nucleoside Therapeutics That Inhibit Human RNRs

The nucleosides F_2C and ClF are used clinically as cancer therapeutics (**Figure 4*b***). F_2C targets a broad spectrum of solid tumors (pancreatic, metastatic breast, lung) and hematological cancers. In the clinic, this compound is used in combination with DNA damaging agents such as cisplatin or small-molecule inhibitors of signaling pathways that affect the cellular response to DNA replication stress (3, 64–66). ClF is limited to hematological cancers (acute myelocytic leukemia, acute lymphocytic leukemia). Both agents inhibit DNA synthesis. RNR is the upstream target of the diphosphate forms of these compounds (F_2CDP, ClFDP), whose inhibition alters dNTP pools. Additionally, the triphosphate forms of these compounds (F_2CTP, ClFTP) inhibit DNA polymerases by incorporation into DNA. The mechanisms by which these compounds inhibit RNR and DNA synthesis, however, are distinct.

F_2CDP

F_2C was synthesized independently by two research groups (58, 67). Studies by Plunkett and colleagues (67–69) demonstrated that F_2C inhibited growth of a variety of tumor cell lines and that cytotoxicity resulted from inhibition of multiple targets, including DNA polymerases and RNR. Biochemical studies on *E. coli* and human RNR established that F_2CDP is a time-dependent irreversible inhibitor and that inactivation occurs with 0.5 equivalent per α subunit. Studies using isotopically labeled F_2CDPs established that the products of the inactivation were distinct depending on whether the inhibition studies were carried out in the presence or in the absence of reductant (70–72).

In the presence of reductant (TR/TRR or DTT) subsequent to cleavage of the 3′ C–H bond of the inhibitor, $2F^-$, cytosine, PP_i, and one alkylated α-cysteine (C_{225}) per α2 were identified, and no Y_{122}• in β2 was lost (**Figure 12*a***). Under these conditions, while only 0.5 equivalents of α are inactivated and β remains active, all enzymatic activity is lost. Analysis of the inhibited reaction mixture by sodium dodecyl sulfate–polyacrylamide gel electrophoresis (SDS-PAGE) with no heating of samples revealed that α migrated as a 60:40 ratio of 80 kDa (endogenous α molecular weight) to 110 kDa (modified α) (**Figure 12*b***). In cancer cell lines incubated with F_2C, SDS-PAGE analysis of cell lysate revealed that the α subunit also migrated in a 60:40 ratio (**Figure 12*b***), similar to what was found in the in vitro studies (73). Similar experiments in the absence of reductant resulted in 50% loss of the β2-Y_{122}• and in the formation of an equivalent amount of a new, nucleotide-based radical (**Figure 12*c***). This radical slowly breaks down to cytosine and PP_i. Inhibition was accompanied by loss of $2F^-$, but the α subunit was not covalently labeled. Thus, in both the presence and absence of reductant, 1 F_2CDP/α2 is sufficient for inhibition, although the underlying mechanisms of inactivation are distinct.

To account for the complete inactivation of RNR with only 0.5 equivalents F_2CDP/α, we proposed that the α/β subunit affinity increased and switching to the second α/β pair for additional chemistry is prevented. To test this possibility, inactivated *E. coli* and human RNR were subjected to size-exclusion chromatography (SEC) analysis. The former showed a species consistent with an apparent molecular weight for α2β2 and the latter with α6β6 (74). In the control, in the absence of F_2CDP, the subunits separate with β eluting as a dimer and α as a mixture of monomers and dimers consistent with weak subunit interactions. On the basis of our recent EM analyses of a mixture of α and β (1:1) with ClFTP (**Figure 6*c***; see also the next section) (27), some α6β2 and no

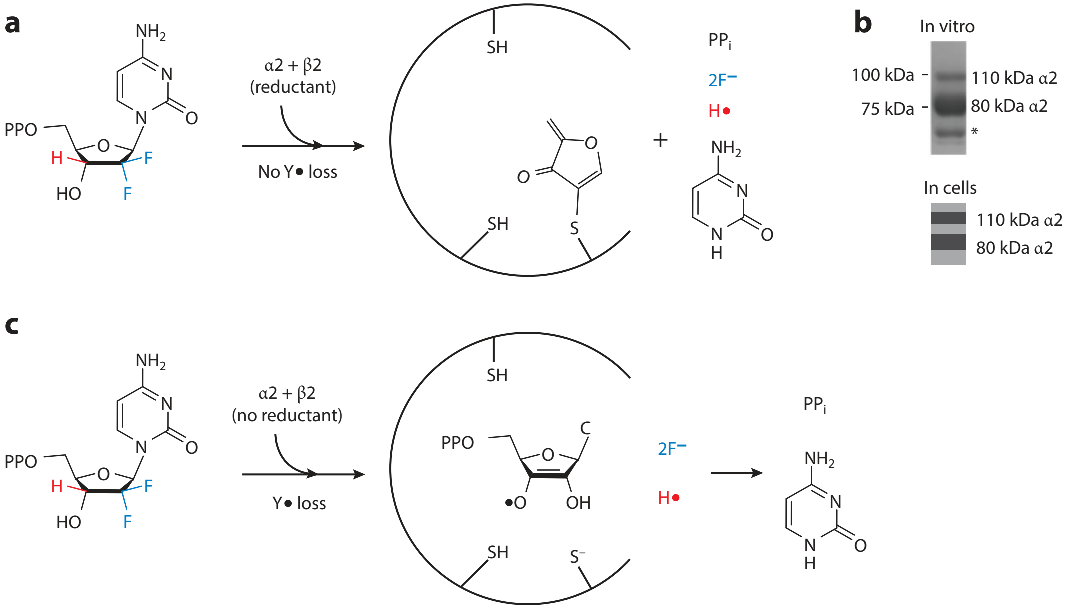

Figure 12

Gemcitabine diphosphate (F_2CDP) (**Figure 4*b***) inhibits human ribonucleotide reductase by distinct mechanisms in (*a*,*b*) the presence and (*c*) the absence of reductant. (*a*) Shown are the products of the inhibition carried out in vitro in the presence of reductant (protein, thioredoxin, or small molecule, dithiothreitol) (70–72). (*b*) SDS-PAGE of RNRs from studies in vitro (*a*) and cell lysate without boiling after incubation with F_2CDP (in vitro) or gemcitabine (F_2C) (in cells; graphic representation of actual data). In vitro and in cell lines (73), α migrates as a 60:40 mixture of an 80-kDa and a 110-kDa α. (*c*) Shown are the products of F_2CDP inhibition carried out in the absence of reductant. Abbreviations: RNR, ribonucleotide reductase; SDS-PAGE, sodium dodecyl sulfate–polyacrylamide gel electrophoresis.

α6β6 was observed. Altered molecular weights using SEC analysis can be attributed to unusual, nonglobular shapes (α6β2) or altered quaternary structure(s). For example, fibril structures have been reported with human α and ATP (27) as well as with *Bacillus subtilis* class Ib (α/β) RNRs (75).

ClFDP and ClFTP (Reversible)

Early studies by Plunkett and colleagues established the toxicity of ClF towards many cell lines (CEM, K562, Hep2). In cell-free systems, ClFTP inhibits RNR and DNA polymerases α and ε (59, 60, 66, 76). The observation that the ClFTP:ClFDP ratio in some cells was 7:1 led to the proposal that ClFTP was a reversible inhibitor of ATP binding to the A site of α (**Figure 2*b***). To better understand how RNR is targeted, kinetic and biochemical studies were undertaken with both ClFDP and ClFTP (61). ClFDP was shown to be a reversible, time-dependent, slow-binding inhibitor of the C site. The kinetic analysis revealed a two-step binding mechanism with a K_I* of 17 nM. ClFTP exhibits reversible, time-independent A-site binding. With ClFTP in five-fold excess relative to RNR under physiological conditions, RNR activity was rapidly and completely lost with a K_I of 40 nM. With sample dilution and follow-up assays, enzyme activity was recovered over 30 min, but only to 50% of the initial value. The half-life ($t_{1/2}$) of human Y• in β2 is 30 min at 37°C (61), and the α subunit is prone to oxidation, making the kinetic measurements challenging; further studies are required. To determine whether the observed inhibition was associated with changes in the RNR's quaternary structure, ClFTP (ClFDP) with α and with and without an allosteric effector (dGTP) were each examined by SEC. In the absence of the corresponding nucleotide in the elution buffer, α migrated as α6 in the presence of either ClFTP or ClFDP. This result is distinct from dATP-α6, which reverts to the monomer when dATP is not present in the elution buffer during SEC. Thus, the presence of ClFDP or ClFTP alters α's quaternary structure such that, even subsequent to ClFD(T)P dissociation, α6 remains trapped in the inactive state. SEC analysis further showed that β2 had no effect on inhibition or migration. Structures of ClFTP mixed with human α/β (1:1) were examined by cryo-EM and solved to 30-Å resolution (**Figure 6*c***). Fewer than one β_2 per three α2 was observed, and it appeared randomly positioned outside or on top of a hexameric ring structure (**Figure 6*c***) (27). In support of this model, experiments with D57N-α in which the mutation in the cone domain prevents hexamerization of α revealed that neither ClFD(T)P-treated mutant RNR nor ClF-treated cells with mutant RNR were inhibited. Finally, *E. coli* RNR, which does not form α6 structures, is not inhibited by ClFDP (61).

The dynamics of quaternary structure interconversions offer an opportunity to inhibit RNRs through unconventional mechanisms. The flexible cone domains (**Figures 2*b*** and **6*a*,*b***) (27, 30) play critical but distinct roles in these states. Strengthening or weakening the interactions responsible for these quaternary structures with small molecules could alter RNR activity.

To assess the importance of the hexameric state of human RNR, investigators studied His_6-α expressed at 3- or 30-fold (3× or 30×) endogenous levels in COS cells that were then treated with noncytotoxic levels of ClF for 3 h. Analysis of the 30× material purified by Ni-affinity chromatography revealed that the α6 state was present; with 3× endogenous levels, cross-linking was required to detect α6. The α6 state from these and other studies is likely the inhibited state inside the cell in the presence of ClFTP and dATP (33).

An extension of this strategy to other adenosine analog therapeutics, ClA and FlU (**Figure 4*b***), has recently been reported (34). In vitro studies of the di- and triphosphates of cladribine (ClADP and ClATP) interactions with human α revealed α6 formation. Further assessment of the hexameric structures and their relationship to cell cytotoxicity is an ongoing challenge. Collectively, results obtained in cells and in vitro with these adenosine inhibitors suggest a potential new way to target RNRs: trapping α in an inhibited state with a small molecule.

Pleiotropic Modes of Cytotoxicity of Gemcitabine and Clofarabine

With both F_2C and ClF, the mechanisms of cytotoxicity require nucleoside uptake and metabolism (64, 65, 77). As noted above, the diphosphates and triphosphates of F_2C and ClF inhibit RNR and DNA polymerases, respectively (60, 78), the latter by chain termination. The consequences of DNA inhibition involving both targets are DNA replication stress that manifests as stalled or collapsed DNA replication forks and DNA single- or double-strand breaks, which can lead to cell cycle arrest, DNA repair, or programmed cell death (64) (**Figure 13**).

F_2CDP, a potent MBI of RNRs, results in lower dNDP and, consequently, dNTP pools. Reduced dCTP, a feedback inhibitor of deoxycytidine kinase (**3**, **Figure 13**), enhances production of F_2CMP, leading to elevated levels of F_2CTP. As a result, F_2CTP can more effectively compete with lowered dNTP pools to inhibit DNA synthesis. F_2C's broad spectrum of solid tumor inhibition, distinct from that of other nucleoside therapeutics such as araC, may be associated with pleiotropic metabolic effects (**Figure 13**), resulting in its self-potentiation (69).

ClF is also phosphorylated by deoxycytidine kinase (**Figure 13**, **3**) and subsequently by distinct kinases to afford ClFDP and ClFTP. Its stability (due to F/Cl substitution) is increased relative to that of other adenosine analogs (ClA, FlU) (**Figure 4*b***) by its resistance to metabolism by purine nucleoside phosphorylase and adenosine deaminase. Downstream consequences of DNA synthesis inhibition by F_2C and ClF are actively being studied. F_2C is being investigated in

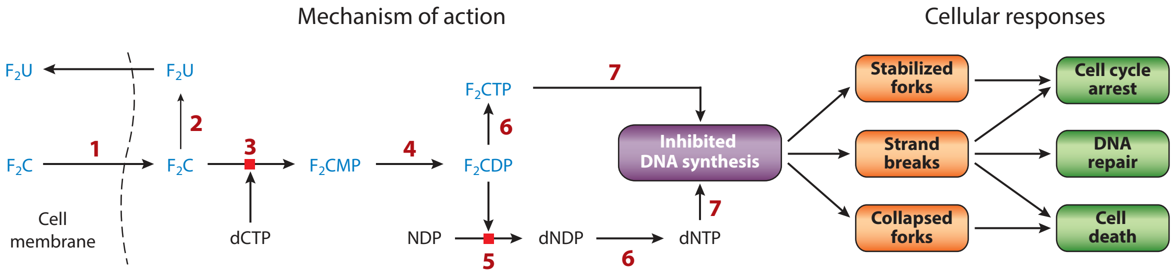

Figure 13

A general scheme for metabolism of nucleosides using gemcitabine (F_2C) as an example (64). F_2C and clofarabine (ClF) therapeutics require cellular uptake and phosphorylation to the appropriate state recognized by target enzymes. The former is mediated by nucleoside transporters ENT1, ENT2, and CNT (**1**). Once inside the cell, both F_2C and ClF are phosphorylated to the monophosphate by deoxycytidine kinase (**3**) and subsequently to the di- and triphosphates by cellular kinases (**4**, **6**). Deoxycytidine kinase has unusual specificity in that it phosphorylates both pyrimidines and purines. The concentrations of the monophosphates are in general greater than the triphosphates and much greater than the diphosphates, are cell type distinct, and influence therapeutic outcomes. (**2**) Cytidine deaminase. (**5**) Ribonucleotide reductase. (**7**) DNA polymerase. Inhibition of DNA synthesis (*purple* box) results in a variety of cellular responses (*orange* and *green* boxes).

combination with DNA damage response inhibitors of checkpoint kinase 1 (Chk1) (64, 68, 79, 80); with inhibitors of ATR, a nuclear kinase that controls S phase progression in response to DNA damage and replication fork stalling, in the same pathway (81); and with DNA repair enzyme inhibitors (65, 82). In addition, F_2C is often used in combination with cisplatin, which enhances DNA damage and alters the downstream consequences. The ability to monitor the consequences of treatment with combinations of therapeutics using genomics, phosphotranscriptomics, and metabolomics has aided and will continue to aid in the development of new approaches (65, 83). For a recent report of alternative functions of h-RNR α and potential effects in therapeutic design, see the sidebar titled A Moonlighting Function of α.

Reversible C-Site Binders Lacking Phosphoryl Groups

Two compounds, I and II (**Figure 14**), have recently been reported to inhibit human RNR by binding reversibly to the C site of α. In contrast to ClFDP and ClADP (**Figure 4*b***), these small molecules lack the diphosphate moiety thought to be essential for substrate recognition. A 5′-substituted amine of F_2C (I), for example, is reported to inhibit RNR in vitro and in vivo (85). The unusual diphosphate binding site for NDP in α (no lysine, arginine, or Mg^{2+}) suggests that amine substitution might avoid issues associated with cellular uptake and phosphorylation (**Figure 13**).

A MOONLIGHTING FUNCTION OF α

A recent report (35) and review (84) provide support for a moonlighting function of α, independent of its ability with β to make dNDP in the cytosol of the cell. Through the use of a C→S mutant that inactivates formation of –S• in α (**Figure 1*a***), a small amount of α was detected in the nucleus of the cell in an α6 state. Yeast two-hybrid experiments with cDNA from HeLa cells revealed that α interacts with ZRANB3, a protein that forms a complex with PCNA, the sliding clamp that, together with DNA polymerase, promotes DNA synthesis in nonstressed cells. Nucleus-localized α inhibits the interaction of ZRANB3 with PCNA, resulting in inhibition of DNA synthesis. This study (35) may explain the tumor suppressor activity reported for α (3).

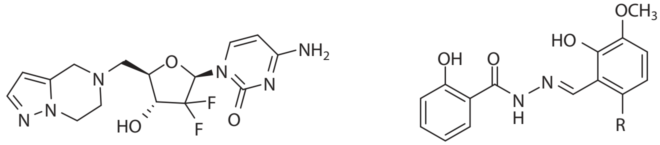

I II

Figure 14

Reversible C-site inhibitors of ribonucleotide reductases lacking phosphoryl groups.

Dealwis and colleagues (86, 87) reported a molecule with a naphthyl salicylic acyl hydrazone scaffold that also targets the C site. Medicinal chemistry approaches to reduce hydrolyzability of the acyl hydrazone and increase interaction with the phosphate binding region led to compound II (**Figure 14**). Decorating the scaffold with an appropriately placed electrophilic moiety such as $ClCH_2CO$-(R″) could result in alkylation of one of the C-site cysteines, analogous to the mechanism of covalent protein kinase inhibitors (88).

Reversible Inhibitors That Disrupt α/β Subunit Affinity

The C-terminal tails (30 to 35 amino acids) of all β2 subunits are disordered (**Figure 2*a***) (18, 89–93), distinct, and predominantly responsible for subunit affinity (**Figure 15**). Early studies of herpes simplex viruses (HSV-1, HSV-2) (94, 95), which encode for their own RNRs, provide an example of how researchers have successfully developed peptidomimetics of their C-terminal tail that disrupted the α/β subunit interface in vitro and in a murine ocular model of HSV-1-induced keratitis (96). The new structure of *E. coli* α2β2 (**Figure 2*d***), which reveals, for the first time, the interaction between the tail (residues 341 to 375) and the α subunit (11), may suggest new ways to disrupt this interface.

A second example of subunit disruption was reported by the Yen group (82, 97), who used the structure of human p53β2 and computer modeling to identify a pocket in each β subunit close to the C-terminal tail but removed from the buried $Fe^{3+}{}_2$-Y• cluster (**Figure 1*c***) essential for β2 stability. Virtual screening and additional experiments led to the identification of COH29 (**Figure 15**), which exhibited cytotoxicity to many of the NIH 60 cancer cell lines and caused S-phase cell cycle arrest. COH29 enhanced cytotoxicity of BRAC1-deficient HCC1937 cells. This

Peptide inhibition of α/β interactions

Organism	C-terminal sequence β
Herpes simplex virus	YAGAVVNDL
Mammals	NSFTLDADF
E. coli	YLVGQIDSEVDTDDLSNFQL
M. tuberculosis	VTEDDDWDF
S. cerevisiae	AGAFTFNEDF

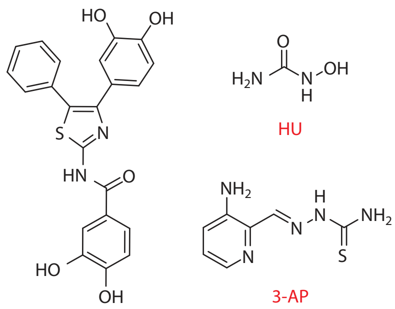

COH29 HU 3-AP

Figure 15

Targeting the α/β interface of active ribonucleotide reductase to prevent active complex formation with peptidomimetics and COH29. Targeting formation and repair of the $M_2{}^{3+}$-Y• (M = Fe; see **Figure 1**) cofactor of β2 with hydroxyurea (HU) and triapine (3-AP).

observation provides an example of DNA repair inhibition (98), in this case genetically, that potentiates the effects of the RNR inhibitor COH29.

BIOSYNTHESIS AND REPAIR OF THE ESSENTIAL DIFERRIC-Y• COFACTOR OF CLASS Ia RNRs: TARGETING THE β2 COFACTOR

Whereas ClF and F_2C target α and the α/β subunits of RNRs, respectively, hydroxyurea (HU) and triapine (3-AP; a thiosemicarbazone) (**Figure 15**) target reduction of the essential Y• cofactor (83, 99, 100) in β2 and/or interfere with cofactor assembly and/or its repair if the essential Y• gets reduced (**Figure 1*c***). HU is used clinically, predominantly in combination with other therapeutics (65), although recent studies have suggested that the RNR is not a key target of its cytotoxicity (99, 101, 102). 3-AP continues to be examined in clinical trials but has not yet been approved for clinical use (83, 100). Although the upstream target of both compounds is the RNR, the downstream pathways that lead to cytotoxicity are pleiotropic and distinct in different organisms. In this section, we focus on HU and 3-AP inhibition of RNRs in vitro and in the early stage of cell culture, when cell viability remains high. Even under these conditions, the detailed mechanism(s) of RNR inhibition requires further exploration.

Background for Metallo-Cluster Metabolism

The class Ia RNRs require a $Fe^{3+}{}_2$-Y• cofactor in β2 to initiate NDP reduction in α2, with activity being directly proportional to the concentration of Y• (**Figures 1*c*** and **3**). The $t_{1/2}$ of the Y• in the cluster of different class Ia β2s is variable, ranging from 4 days in *E. coli* at 4°C to 30 min in humans at 37°C. In addition, recombinant expression of β from different organisms results in variable amounts of active cofactor (0 to 1 $Fe^{3+}{}_2$-Y•/β2) (6, 103). In general, therefore, the β2 cofactor must be loaded by self-assembly by use of $Fe^{2+}$and O_2, with variable outcomes (6, 104). In the past 2 decades, the importance of biosynthetic pathways has been established for FeS cluster cofactor assembly that, in turn, has been linked to formation of mono- and dinuclear nonheme iron cofactors, including the RNR cofactor (105). Although much remains to be learned, genetic studies in *E. coli* and *S. cerevisiae*, as well as in vitro biochemical studies on these class Ia β2s, suggest that there are pathways not only for cofactor biosynthesis but also for its maintenance and activity regulation (**Figure 16**). Our general model for $Fe^{3+}{}_2$-Y• cofactor biosynthesis indicates a requirement for one or more chaperone proteins (106) to alter the apo-β2 conformation for optimized Fe^{2+} loading, an Fe^{2+} carrier protein or small molecule that delivers Fe^{2+} to apo-β2, and a reducing equivalent delivery mechanism required for cluster assembly with O_2 as the oxidant (107). Studies in vivo in *E. coli* (108) and *S. cerevisiae* (109) reveal that cluster assembly can yield β2 in which each β subunit has two Fe^{3+} and one Y•, that is, quantitative loading. In vitro, however, *E. coli* β2 loading gives rise to ∼66% active cofactor and 34% inactive diferric clusters with no Y•. In both in vivo and in vitro loading, the activity of the RNR per Y• is the same, suggesting identical cofactor structures.

Hydroxyurea

HU (**Figure 15**) has been studied since the 1960s. On the basis of EPR analyses of prokaryotic and eukaryotic cells and of purified β2 with a self-assembled $Fe^{3+}{}_2$-Y•, HU treatment reduces Y• to YOH. In vitro, the iron cluster of human β2 is also reduced ($Fe^{2+}{}_2$-YOH), whereas in *E. coli* it remains in the Fe^{3+} state ($Fe^{3+}{}_2$-YOH). HU reduction of β2 alone is slow (0.45 M^{-1} s^{-1}), and there is no evidence that it binds to either *E. coli* or human β2 (107, 110, 111). The chemical mechanism of Y• reduction and the structure of the resulting cluster remain unknown (112). An

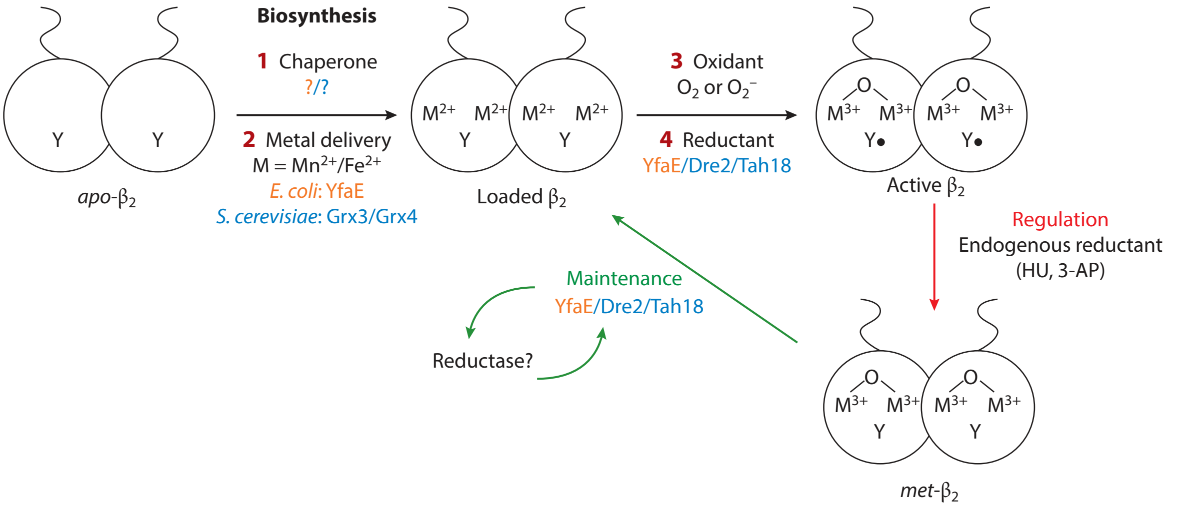

Figure 16

Model for Me_2^{3+}-Y• (Me = Fe or Mn) cofactor biosynthesis (*black*), maintenance (*green*), and regulation (*red*). Factors identified from *Escherichia coli* are in orange, and those from *Saccharomyces cerevisiae* are in blue (6). *S. cerevisiae* counterparts are found in humans. Regulation can occur by endogenous reductants or by therapeutics such as hydroxyurea (HU) and triapine (3-AP) (see **Figure 15**).

in vitro study by the Sjöberg laboratory (113) has shown that HU-mediated loss of RNR activity is potentiated 10-fold by complexation of β2 with α2, substrate, and effector. This result led these authors to suggest that HU reduction of Y_{122}• is not direct but rather might involve trapping of a transient pathway radical at the α/β subunit interface (**Figure 3**). Studies of the reduction by HU of the $Mn^{4+}Fe^{3+}$-β2 cofactor in the *Chlamydia trachomatis* class Ic RNR (**Figure 1*c***), an Fe^{3+}_2-Y• surrogate, were also interpreted to suggest that HU intercepts a pathway radical at the α/β subunit interface (112). Furthermore, in the presence of α2, CDP, and ATP, $Mn^{4+}Fe^{3+}$-β2 is reduced by HU to an Mn^{3+}–Fe^{3+} cluster with half-site reactivity involving a fast phase and a slow phase, with apparent saturation by HU for the fast phase. These studies support HU binding and targeting of the RT pathway (112, 114). The consequences of the HU-reduced cofactor state in *E. coli* and mammalian cells are still unclear; however, since the proteins identified in *S. cerevisiae* for β2 cofactor biosynthesis and maintenance are also found in mammalian cells (107), Y• regeneration is a possible fate (**Figure 16**) and requires further investigation.

RNR inhibition by HU blocks DNA replication**.** Two papers have suggested that cytotoxicity from extended HU exposure of *E. coli* (101) or *S. cerevisiae* (102) cells is linked to reactive oxygen species (such as HO•)-mediated damage. Vernis and colleagues (102) have shown that HU resistance in *S. cerevisiae* leads to enhanced production of the cytosolic FeS cluster biosynthetic machinery, including Dre2/Tah18. We have demonstrated the importance of these two proteins in the assembly of the β2 cofactor in *S. cerevisiae* (107).

Triapine

3-AP (**Figure 15**) has been extensively investigated since its introduction in the 1990s, and its cytotoxic effects have inspired the synthesis of many additional thiosemicarbazones. However, studies of these analogs reveal that the mechanism of cytotoxicity changes with structure. The complexity arises from their distinct abilities to bind Fe^{2+} and Fe^{3+} (as well as Cu^{2+} and Zn^{2+}) and the resultant ligand field–imposed iron redox chemistry (100). Results reported by different groups (115, 116) in different mammalian cell lines, primarily at late stages of 3-AP treatment, have thus made it challenging to compare and evaluate the outcomes of the different studies.

Our recent studies in cell culture in the early stages of 3-AP treatment provide a framework for thinking about the issues and evaluating its potential as a therapeutic that targets β2 (115). Three mammalian cell lines (K565, COS-1, and HU-resistant TA3) treated with 3-AP and analyzed by whole-cell EPR revealed loss of the RNR Y•, and assays of the corresponding cell lysates revealed loss of RNR activity. Immunoprecipitation of β2 from ^{55}Fe-treated and nontreated cells revealed similar iron content. These and additional studies suggest that Y• loss is the major mode of RNR inhibition, with iron loading remaining unchanged. Although the oxidation state of the bound iron is unknown, we know from in vitro studies that Fe^{2+}-loaded β2 can assemble rapidly into the native $Fe^{3+}{}_2$-Y• cofactor, consistent with a maintenance pathway (**Figure 16**). In our model, Fe^{2+}-(3-AP) is the active species involved in β2 inhibition, and in the continued presence of Fe^{2+}/Fe^{3+}, the RNR is susceptible to Fe^{2+}-(3-AP) inhibition by direct Y• reduction. In a recent study by Gräslund and colleagues (116), the use of [^{3}H]-(3-AP) and a docking model of 3-AP to mouse β2 resulted in the proposal of a specific 3-AP binding site. However, neither 3-AP nor Fe^{2+}-(3-AP) binding to β2 has been observed. In our opinion, the mechanism of action of these compounds requires further study. Finally, our studies at early stages subsequent to 3-AP treatment, in contrast to other researchers' later-stage studies, indicate that reactive oxygen species are not responsible for loss of RNR activity.

How 3-AP and HU inhibit RNR and the nature of the relationship between their RNR inhibition and cell cytotoxicity remain a mystery. Although interference with cluster assembly and maintenance might yield effective therapeutics, a better understanding of the biology of $Fe^{3+}{}_2$-Y• pathways is required. However, the recent discovery of $Mn^{3+}{}_2$-Y• cofactors in β2 of class Ib RNRs (**Figure 1*c***) and the identification of a NrdI-β2 interaction essential for both oxidant delivery ($O_2^{\bullet -}$) and active cofactor formation (**Figure 16**) (6, 117) suggest that disruption of this protein/protein interface could provide proof of principle for targeting of cofactor pathways in pathogenic bacteria. The link among the class Ia $Fe^{3+}{}_2$-Y• pathway, iron homeostasis, and oxidative stress will make selective targeting difficult. However, for pathogenic organisms with Mn and or Mn/Fe clusters (**Figure 1*c***), interference with cluster assembly may well provide a new therapeutic target.

SUMMARY POINTS

1. The quaternary structures of the class Ia RNR α subunit are nucleotide dependent and distinct. The α structures detected to date are α, α2, noncanonical α2 (118), α4, α6, and fibrils (27, 75).
2. dATP-inhibited RNR structures include α6 (human), α4β4 (*E. coli*), α4 (*Pseudomonas aeruginosa*) (119), and a double-helical fibril of canonical and noncanonical α2s (class Ib; *B. subtilis*) (75).
3. dATP-inhibited states appear to interfere with the RT pathway and –S• formation by preventing β2 from forming a productive α2β2 complex.
4. ClFDP (ClFTP) binds to human RNR and forms conformationally stable α6 state(s), even after dissociation.
5. N_3NDP and F_2CDP are mechanism-based inhibitors of class Ia RNRs with one inhibitor/α2 in the α2β2 complex, half-site reactivity.

6. Incorporation of unnatural amino acids (F_3Y_{122}• or NO_2Y_{122}• to replace Y_{122}• in β or NH_2Y to replace three residues: Y_{356} in β, Y_{731} in α, or Y_{730} in α) and incubation with the second subunit, substrate, and effector trap radicals within the pathway and increases α/β subunit affinity.
7. The reaction of F_3Y_{122}•/E52Q-β2 with α2, substrate, and effector results in an asymmetric, active, and kinetically trapped α2β2 complex, whose structure has been determined by cryo-EM (11). The RT pathway is revealed for the first time as is the C-terminal tail of one β2 bound to α2.

FUTURE ISSUES

1. Trapping of additional α2β2 complexes of RNRs using mechanism-based inhibitors and unnatural amino acid mutants to trap radicals in a forward or reverse radical transfer pathway may provide distinct and higher-resolution structures.
2. Cryo-EM analyses have shown that the active form of a mutant *E. coli* class Ia RNR is an asymmetric and dynamic α2β2. The relationship of this structure to the wild-type enzyme and the structure of the human active complex remain to be established.
3. Identification of small molecules that can trap human and bacterial RNRs in distinct inhibited quaternary structures represents a new way to target RNRs.
4. The discovery of biosynthetic pathways for dimetallo-Y• cluster assembly in class Ia and Ib RNRs suggests that targeting the metal center formation, such as disruption of NrdI/NrdF interaction in the assembly of the class Ib $Mn^{3+}{}_2$-Y• cofactor, might be possible.
5. The omics revolution (proteomics, phosphomics, transcriptomics) and a refined understanding of nucleotide metabolism are providing new insight into RNR regulation. This knowledge will lead to combination chemotherapies using RNR inhibitors in conjunction with inhibitors of downstream signaling pathways.

DISCLOSURE STATEMENT

The authors are not aware of any affiliations, memberships, funding, or financial holdings that might be perceived as affecting the objectivity of this review.

ACKNOWLEDGMENTS

We acknowledge the following funding sources: NIH grant GM29595 (J.S.); NIH grant GM126982 (C.L.D.); David H. Koch Graduate Fellowship (G.K.); C.L.D. is an HHMI investigator; and NIH grant GM472274 (D.G.N.). J.S., D.G.N., C.L.D., and M.B. thank all of their coworkers for their contributions to understanding RNRs.

LITERATURE CITED

1. Hofer A, Crona M, Logan DT, Sjöberg BM. 2012. DNA building blocks: keeping control of manufacture. *Crit. Rev. Biochem. Mol. Biol.* 47:50–63

2. Guarino E, Salguero I, Kearsey SE. 2014. Cellular regulation of ribonucleotide reductase in eukaryotes. *Semin. Cell Dev. Biol.* 30:97–103
3. Aye Y, Li M, Long MJC, Weiss RS. 2014. Ribonucleotide reductase and cancer: biological mechanisms and targeted therapies. *Oncogene* 34:2011–21
4. Le TM, Poddar S, Capri JR, Abt ER, Kim W, et al. 2017. ATR inhibition facilitates targeting of leukemia dependence on convergent nucleotide biosynthetic pathways. *Nat. Commun.* 8:241
5. Licht S, Stubbe J. 1999. Mechanistic investigations of ribonucleotide reductases. In *Enzymes, Enzyme Mechanisms, and Aspects of NO Chemistry*, ed. CD Poulter, pp. 163–203. Compr. Nat. Prod. Chem. Vol. 5. Kidlington, UK: Pergamon Press
6. Cotruvo JA, Stubbe J. 2011. Class I ribonucleotide reductases: metallocofactor assembly and repair in vitro and in vivo. *Annu. Rev. Biochem.* 80:733–67
7. Minnihan EC, Nocera DG, Stubbe J. 2013. Reversible, long-range radical transfer in *E. coli* class Ia ribonucleotide reductase. *Acc. Chem. Res.* 46:2524–35
8. Fairman JW, Wijerathna SR, Ahmad MF, Xu H, Nakano R, et al. 2011. Structural basis for allosteric regulation of human ribonucleotide reductase by nucleotide-induced oligomerization. *Nat. Struct. Mol. Biol.* 18:316–22
9. Bennati M, Weber A, Antonic J, Perlstein DL, Robblee JH, Stubbe J. 2003. Pulsed ELDOR spectroscopy measured the distance between the two tyrosyl radicals in the R2 subunit of the *E. coli* ribonucleotide reductase. *J. Am. Chem. Soc.* 125:14988–89
10. Seyedsayamdost MR, Chan CTY, Mugnaini V, Stubbe J, Bennati M. 2007. PELDOR spectroscopy with DOPA-β2 and NH_2Y-α2s: distance measurements between residues involved in the radical propagation pathway of *E. coli* ribonucleotide reductase. *J. Am. Chem. Soc.* 129:15748–49
11. Kang G, Taguchi AT, Stubbe J, Drennan CL. 2020. Structure of a trapped radical transfer pathway within a ribonucleotide reductase holocomplex. *Science* 368:424–27
12. Zimanyi CM, Chen PY, Kang G, Funk MA, Drennan CL. 2016. Molecular basis for allosteric specificity regulation in class Ia ribonucleotide reductase from *Escherichia coli*. *eLife* 5:e07141
13. Uhlin U, Eklund H. 1994. Structure of ribonucleotide reductase protein R1. *Nature* 370:533–39
14. Stubbe J. 1998. Ribonucleotide reductases in the twenty-first century. *PNAS* 95:2723–24
15. Stubbe J, Seyedsayamdost MR. 2019. Discovery of a new class I ribonucleotide reductase with an essential DOPA radical and NO metal as an initiator of long-range radical transfer. *Biochemistry* 58:435–37
16. Srinivas V, Lebrette H, Lundin D, Kutin Y, Sahlin M, et al. 2018. Metal-free ribonucleotide reduction powered by a DOPA radical in *Mycoplasma* pathogens. *Nature* 563:416–20
17. Blaesi EJ, Palowitch GM, Hu K, Kim AJ, Rose HR, et al. 2018. Metal-free class Ie ribonucleotide reductase from pathogens initiates catalysis with a tyrosine-derived dihydroxyphenylalanine radical. *PNAS* 115:10022–27
18. Eklund H, Uhlin U, Färnegårdh M, Logan DT, Nordlund P. 2001. Structure and function of the radical enzyme ribonucleotide reductase. *Prog. Biophys. Mol. Biol.* 77:177–268
19. Nordlund P, Sjöberg BM, Eklund H. 1990. Three-dimensional structure of the free radical protein of ribonucleotide reductase. *Nature* 345:593–98
20. Jordan A, Reichard P. 1998. Ribonucleotide reductases. *Annu. Rev. Biochem.* 67:71–98
21. Nordlund P, Reichard P. 2006. Ribonucleotide reductases. *Annu. Rev. Biochem.* 75:681–706
22. Ge J, Yu G, Ator MA, Stubbe J. 2003. Pre-steady-state and steady-state kinetic analysis of *E. coli* class I ribonucleotide reductase. *Biochemistry* 42:10071–83
23. Ravichandran KR, Taguchi AT, Wei Y, Nocera DG, Stubbe J. 2016. A >200 meV uphill thermodynamic landscape for radical transport in *E. coli* ribonucleotide reductase determined using fluorotyrosine-substituted enzymes. *J. Am. Chem. Soc.* 138:13706–16
24. Ravichandran KR, Zong AB, Taguchi AT, Nocera DG, Stubbe J, Tommos C. 2017. Formal reduction potentials of difluorotyrosine and trifluorotyrosine protein residues: defining the thermodynamics of multistep radical transfer. *J. Am. Chem. Soc.* 139:2994–3004
25. Minnihan EC, Ando N, Brignole EJ, Olshansky L, Chittuluru J, et al. 2013. Generation of a stable, aminotyrosyl radical-induced α2β2 complex of *Escherichia coli* class Ia ribonucleotide reductase. *PNAS* 110:3835–40

26. Yokoyama K, Smith AA, Corzilius B, Griffin RG, Stubbe J. 2011. Equilibration of tyrosyl radicals (Y356•, Y731•, Y730•) in the radical propagation pathway of the *Escherichia coli* class Ia ribonucleotide reductase. *J. Am. Chem. Soc.* 133:18420–32
27. Brignole EJ, Tsai K-L, Chittuluru J, Li H, Aye Y, et al. 2018. 3.3-Å resolution cryo-EM structure of human ribonucleotide reductase with substrate and allosteric regulators bound. *eLife* 7:e31502
28. Ando N, Li H, Brignole EJ, Thompson S, McLaughlin MI, et al. 2016. Allosteric inhibition of human ribonucleotide reductase by dATP entails the stabilization of a hexamer. *Biochemistry* 55:373–81
29. Ando N, Brignole EJ, Zimanyi CM, Funk MA, Yokoyama K, et al. 2011. Structural interconversions modulate activity of *Escherichia coli* ribonucleotide reductase. *PNAS* 108:21046–51
30. Zimanyi CM, Ando N, Brignole EJ, Asturias FJ, Stubbe J, Drennan CL. 2012. Tangled up in knots: structures of inactivated forms of *E. coli* class Ia ribonucleotide reductase. *Structure* 20:1374–83
31. Chen PY, Funk MA, Brignole EJ, Drennan CL. 2018. Disruption of an oligomeric interface prevents allosteric inhibition of *Escherichia coli* class Ia ribonucleotide reductase. *J. Biol. Chem.* 293:10404–12
32. Ahluwalia D, Bienstock RJ, Schaaper RM. 2012. Novel mutator mutants of *E. coli* nrdAB ribonucleotide reductase: insight into allosteric regulation and control of mutation rates. *DNA Repair* 11:480–87
33. Aye Y, Brignole EJ, Long MJ, Chittuluru J, Drennan CL, et al. 2012. Clofarabine targets the large subunit (α) of human ribonucleotide reductase in live cells by assembly into persistent hexamers. *Chem. Biol.* 19:799–805
34. Wisitpitthaya S, Zhao Y, Long MJC, Li M, Fletcher EA, et al. 2016. Cladribine and fludarabine nucleotides induce distinct hexamers defining a common mode of reversible RNR inhibition. *ACS Chem. Biol.* 11:2021–32
35. Fu Y, Long MJC, Wisitpitthaya S, Inayat H, Pierpont TM, et al. 2018. Nuclear RNR-α antagonizes cell proliferation by directly inhibiting ZRANB3. *Nat. Chem. Biol.* 14:943–54
36. Lin Q, Parker MJ, Taguchi AT, Ravichandran K, Kim A, et al. 2017. Glutamate 52-β at the α/β subunit interface of *Escherichia coli* class Ia ribonucleotide reductase is essential for conformational gating of radical transfer. *J. Biol. Chem.* 292:9229–39
37. Erickson HK. 2001. Kinetics in the pre-steady state of the formation of cystines in ribonucleoside diphosphate reductase: evidence for an asymmetric complex. *Biochemistry* 40:9631–37
38. Lou M, Liu Q, Ren GP, Zeng JL, Xiang XP, et al. 2017. Physical interaction between human ribonucleotide reductase large subunit and thioredoxin increases colorectal cancer malignancy. *J. Biol. Chem.* 292:9136–49
39. Makhlynets O, Boal AK, Rhodes DV, Kitten T, Rosenzweig AC, Stubbe J. 2014. *Streptococcus sanguinis* class Ib ribonucleotide reductase: high activity with both iron and manganese cofactors and structural insights. *J. Biol. Chem.* 289:6259–72
40. Lu J, Holmgren A. 2014. The thioredoxin antioxidant system. *Free Radic. Biol. Med.* 66:75–87
41. Parker MJ, Stubbe J. 2014. *Bacillus subtilis* class Ib ribonucleotide reductase: high activity and dynamic subunit interactions. *Biochemistry* 53:766–76
42. Ravichandran KR, Olshansky L, Nocera DG, Stubbe J. 2020. Subunit interaction dynamics of class Ia ribonucleotide reductases: in search of a robust assay. *Biochemistry* 59:1442–53
43. Stubbe J, van der Donk WA. 1998. Protein radicals in enzyme catalysis. *Chem. Rev.* 98:705–62
44. Stubbe J, Ackles D. 1980. On the mechanism of ribonucleoside diphosphate reductase from *Escherichia coli*. Evidence for 3′-C–H bond cleavage. *J. Biol. Chem.* 255:8027–30
45. Lenz R, Giese B. 1997. Studies on the mechanism of ribonucleotide reductases. *J. Am. Chem. Soc.* 119:2784–94
46. Licht SS, Booker S, Stubbe J. 1999. Studies on the catalysis of carbon-cobalt bond homolysis by ribonucleoside triphosphate reductase: evidence for concerted carbon-cobalt bond homolysis and thiyl radical formation. *Biochemistry* 38:1221–33
47. Licht S, Gerfen GJ, Stubbe J. 1996. Thiyl radicals in ribonucleotide reductases. *Science* 271:477–81
48. Lawrence CC, Bennati M, Obias HV, Bar G, Griffin RG, Stubbe J. 1999. High-field EPR detection of a disulfide radical anion in the reduction of cytidine 5′-diphosphate by the E_{441}Q-R1 mutant of *Escherichia coli* ribonucleotide reductase. *PNAS* 96:8979–84

49. Pizano AA, Lutterman DA, Holder PG, Teets TS, Stubbe J, Nocera DG. 2011. Photo-ribonucleotide reductase β2 by selective cysteine labeling with a radical phototrigger. *PNAS* 109:39–43
50. Chang MCY, Yee CS, Stubbe J, Nocera DG. 2004. Turning on ribonucleotide reductase by light-initiated amino acid radical generation. *PNAS* 101:6882–87
51. Olshansky L, Pizano AA, Wei Y, Stubbe J, Nocera DG. 2014. Kinetics of hydrogen atom abstraction from substrate by an active site thiyl radical in ribonucleotide reductase. *J. Am. Chem. Soc.* 136:16210–16
52. Licht SS, Lawrence CC, Stubbe J. 1999. Class II ribonucleotide reductases catalyze carbon-cobalt bond reformation on every turnover. *J. Am. Chem. Soc.* 121:7463–68
53. Stubbe J, van der Donk WA. 1995. Ribonucleotide reductases: radical enzymes with suicidal tendencies. *Chem. Biol.* 2:793–801
54. Thelander L, Larsson B, Hobbs J, Eckstein F. 1976. Active site of ribonucleoside diphosphate reductase from *Escherichia coli*. *J. Biol. Chem.* 251:1396–405
55. van der Donk WA, Yu G, Silva DJ, Stubbe J, McCarthy JR, et al. 1996. Inactivation of ribonucleotide reductase by (E)-2′-fluoromethylene-2′-deoxycytidine 5′-diphosphate: a paradigm for nucleotide mechanism-based inhibitors. *Biochemistry* 35:8381–91
56. Bitonti AJ, Dumont JA, Bush TL, Cashman EA, Cross-Doersen DE, et al. 1994. Regression of human breast tumor xenografts in response to (E)-2′-deoxy-2′-(fluoromethylene)cytidine, an inhibitor of ribonucleoside diphosphate reductase. *Cancer Res.* 54:1485–90
57. Zhou Y, Achanta G, Pelicano H, Gandhi V, Plunkett W, Huang P. 2002. Action of (E)-2′-deoxy-2′-(fluoromethylene)cytidine on DNA metabolism: incorporation, excision, and cellular response. *Mol. Pharmacol.* 61:222–29
58. Baker CH, Banzon J, Bollinger JM, Stubbe J, Samano V, et al. 1991. 2′-Deoxy-2′-methylenecytidine and 2′-deoxy-2′,2′-difluorocytidine 5′-diphosphates: potent mechanism-based inhibitors of ribonucleotide reductase. *J. Med. Chem.* 34:1879–84
59. Xie KC, Plunkett W. 1996. Deoxynucleotide pool depletion and sustained inhibition of ribonucleotide reductase and DNA synthesis after treatment of human lymphoblastoid cells with 2-chloro-9-(2-deoxy-2-fluoro-β-D-arabinofuranosyl) adenine. *Cancer Res.* 56:3030–37
60. Xie C, Plunkett W. 1995. Metabolism and actions of 2-chloro-9-(2-deoxy-2-fluoro-β-D-arabinofuranosyl)-adenine in human lymphoblastoid cells. *Cancer Res.* 55:2847–52
61. Aye Y, Stubbe J. 2011. Clofarabine 5′-di and -triphosphates inhibit human ribonucleotide reductase by altering the quaternary structure of its large subunit. *PNAS* 108:9815–20
62. Fritscher J, Artin E, Wnuk S, Bar G, Robblee JH, et al. 2005. Structure of the nitrogen-centered radical formed during inactivation of *E. coli* ribonucleotide reductase by 2′-azido-2′-deoxyuridine-5′-diphosphate: trapping of the 3′-ketonucleotide. *J. Am. Chem. Soc.* 127:7729–38
63. Sjöberg BM, Gräslund A, Eckstein F. 1983. A substrate radical intermediate in the reaction between ribonucleotide reductase from *Escherichia coli* and 2′-azido-2′-deoxynucleoside diphosphates. *J. Biol. Chem.* 258:8060–67
64. Ewald B, Sampath D, Plunkett W. 2008. Nucleoside analogs: molecular mechanisms signaling cell death. *Oncogene* 27:6522–37
65. Murai J. 2017. Targeting DNA repair and replication stress in the treatment of ovarian cancer. *Int. J. Clin. Oncol.* 22:619–28
66. Bonate PL, Arthaud L, Cantrell WR Jr., Stephenson K, Secrist JA, Weitman S. 2006. Discovery and development of clofarabine: a nucleoside analogue for treating cancer. *Nat. Rev. Drug Discov.* 5:855–63
67. Hertel LW, Boder GB, Kroin JS, Rinzel SM, Poore GA, et al. 1990. Evaluation of the antitumor activity of gemcitabine (2′,2′-difluoro-2′-deoxycytidine). *Cancer Res.* 50:4417–22
68. Ewald B, Sampath D, Plunkett W. 2007. H2AX phosphorylation marks gemcitabine-induced stalled replication forks and their collapse upon S-phase checkpoint abrogation. *Mol. Cancer Ther.* 6:1239–48
69. Plunkett W, Huang P, Searcy CE, Gandhi V. 1996. Gemcitabine: preclinical pharmacology and mechanisms of action. *Semin. Oncol.* 23:3–15
70. van der Donk WA, Yu GX, Pérez L, Sanchez RJ, Stubbe J, et al. 1998. Detection of a new substrate-derived radical during inactivation of ribonucleotide reductase from *Escherichia coli* by gemcitabine 5′-diphosphate. *Biochemistry* 37:6419–26

71. Artin E, Wang J, Lohman GJ, Yokoyama K, Yu G, et al. 2009. Insight into the mechanism of inactivation of ribonucleotide reductase by gemcitabine 5′-diphosphate in the presence or absence of reductant. *Biochemistry* 48:11622–29
72. Wang J, Lohman GJ, Stubbe J. 2009. Mechanism of inactivation of human ribonucleotide reductase with p53R2 by gemcitabine 5′-diphosphate. *Biochemistry* 48:11612–21
73. Chen Z, Zhou J, Zhang Y, Bepler G. 2011. Modulation of the ribonucleotide reductase M1-gemcitabine interaction in vivo by *N*-ethylmaleimide. *Biochem. Biophys. Res. Commun.* 413:383–88
74. Wang J, Lohman GJ, Stubbe J. 2007. Enhanced subunit interactions with gemcitabine-5′-diphosphate inhibit ribonucleotide reductases. *PNAS* 104:14324–29
75. Thomas WC, Brooks FP, Burnim AA, Bacik JP, Stubbe J, et al. 2019. Convergent allostery in ribonucleotide reductase. *Nat. Commun.* 10:2653
76. Ghanem H, Jabbour E, Faderl S, Ghandhi V, Plunkett W, Kantarjian H. 2010. Clofarabine in leukemia. *Expert Rev. Hematol.* 3:15–22
77. Wong A, Soo RA, Yong WP, Innocenti F. 2009. Clinical pharmacology and pharmacogenetics of gemcitabine. *Drug Metab. Rev.* 41:77–88
78. Xie C, Plunkett W. 1995. Metabolism and actions of 2-chloro-9-(2-deoxy-2-fluoro-β-D-arabinofuranosyl)-adenine in human lymphoblastoid cells. *Cancer Res.* 55:2847–52
79. Warren NJH, Eastman A. 2019. Inhibition of checkpoint kinase 1 following gemcitabine-mediated S phase arrest results in CDC7- and CDK2-dependent replication catastrophe. *J. Biol. Chem.* 294:1763–78
80. Liu Y, Li Y, Wang X, Liu F, Gao P, et al. 2017. Gemcitabine and Chk1 inhibitor AZD7762 synergistically suppress the growth of Lkb1-deficient lung adenocarcinoma. *Cancer Res.* 77:5068–76
81. Fordham SE, Blair HJ, Elstob CJ, Plummer R, Drew Y, et al. 2018. Inhibition of ATR acutely sensitizes acute myeloid leukemia cells to nucleoside analogs that target ribonucleotide reductase. *Blood Adv.* 2:1157–69
82. Chen YR, Tsou B, Hu S, Ma H, Liu X, et al. 2016. Autophagy induction causes a synthetic lethal sensitization to ribonucleotide reductase inhibition in breast cancer cells. *Oncotarget* 7:1984–99
83. Mannargudi MB, Deb S. 2017. Clinical pharmacology and clinical trials of ribonucleotide reductase inhibitors: Is it a viable cancer therapy? *J. Cancer Res. Clin. Oncol.* 143:1499–529
84. Long MJC, Van Hall-Beauvais A, Aye Y. 2019. The more the merrier: how homo-oligomerization alters the interactome and function of ribonucleotide reductase. *Curr. Opin. Chem. Biol.* 54:10–18
85. Labroli MA, Dwyer MP, Shen R, Popovici-Muller J, Pu Q, et al. 2014. The identification of novel 5′-amino gemcitabine analogs as potent RRM1 inhibitors. *Bioorg. Med. Chem.* 22:2303–10
86. Misko TA, Liu YT, Harris ME, Oleinick NL, Pink J, et al. 2019. Structure-guided design of anti-cancer ribonucleotide reductase inhibitors. *J. Enzym. Inhib. Med. Chem.* 34:438–50
87. Ahmad MF, Alam I, Huff SE, Pink J, Flanagan SA, et al. 2017. Potent competitive inhibition of human ribonucleotide reductase by a nonnucleoside small molecule. *PNAS* 114:8241–46
88. Backus KM, Cao J, Maddox SM. 2019. Opportunities and challenges for the development of covalent chemical immunomodulators. *Bioorg. Med. Chem.* 27:3421–39
89. Moss N, Beaulieu P, Duceppe JS, Ferland JM, Gauthier J, et al. 1995. Peptidomimetic inhibitors of herpes simplex virus ribonucleotide reductase: a new class of antiviral agents. *J. Med. Chem.* 38:3617–23
90. Climent I, Sjöberg BM, Huang CY. 1991. Carboxyl-terminal peptides as probes for *Escherichia coli* ribonucleotide reductase subunit interaction: kinetic analysis of inhibition studies. *Biochemistry* 30:5164–71
91. Climent I, Sjöberg BM, Huang CY. 1992. Site-directed mutagenesis and deletion of the carboxyl terminus of *Escherichia coli* ribonucleotide reductase protein R2—effects on catalytic activity and subunit interaction. *Biochemistry* 31:4801–7
92. Xu H, Fairman JW, Wijerathna SR, Kreischer NR, LaMacchia J, et al. 2008. The structural basis for peptidomimetic inhibition of eukaryotic ribonucleotide reductase: a conformationally flexible pharmacophore. *J. Med. Chem.* 51:4653–59
93. Cooperman BS, Gao Y, Tan C, Kashlan OB, Kaur J. 2005. Peptide inhibitors of mammalian ribonucleotide reductase. *Adv. Enzym. Regul.* 45:112–25

94. Cohen EA, Gaudreau P, Brazeau P, Langelier Y. 1986. Specific inhibition of herpesvirus ribonucleotide reductase by a nonapeptide derived from the carboxy terminus of subunit 2. *Nature* 321:441–43
95. Dutia BM, Frame MC, Subak-Sharpe JH, Clark WN, Marsden HS. 1986. Specific inhibition of herpesvirus ribonucleotide reductase by synthetic peptides. *Nature* 321:439–41
96. Liuzzi M, Déziel R, Moss N, Beaulieu P, Bonneau A-M, et al. 1994. A potent peptidomimetic inhibitor of HSV ribonucleotide reductase with antiviral activity in vivo. *Nature* 372:695–98
97. Zhou B, Su L, Hu S, Hu W, Yip ML, et al. 2013. A small-molecule blocking ribonucleotide reductase holoenzyme formation inhibits cancer cell growth and overcomes drug resistance. *Cancer Res*. 73:6484–93
98. Chen MC, Zhou B, Zhang K, Yuan YC, Un F, et al. 2015. The novel ribonucleotide reductase inhibitor COH29 inhibits DNA repair in vitro. *Mol. Pharmacol.* 87:996–1005
99. Singh A, Xu YJ. 2016. The cell killing mechanisms of hydroxyurea. *Genes* 7:99
100. Heffeter P, Pape VF, Enyedy EA, Keppler BK, Szakacs G, Kowol CR. 2019. Anticancer thiosemicarbazones: chemical properties, interaction with iron metabolism, and resistance development. *Antioxid. Redox Signal.* 30:1062–82
101. Davies BW, Kohanski MA, Simmons LA, Winkler JA, Collins JJ, Walker GC. 2009. Hydroxyurea induces hydroxyl radical–mediated cell death in *Escherichia coli*. *Mol. Cell* 36:845–60
102. Huang ME, Facca C, Fatmi Z, Baille D, Benakli S, Vernis L. 2016. DNA replication inhibitor hydroxyurea alters Fe-S centers by producing reactive oxygen species in vivo. *Sci. Rep.* 6:29361
103. Stubbe J, Cotruvo JA. 2011. Control of metallation and active cofactor assembly in the class Ia and Ib ribonucleotide reductases: diiron or dimanganese? *Curr. Opin. Chem. Biol.* 15:284–90
104. Atkin CL, Thelander L, Reichard P, Lang G. 1973. Iron and free radical in ribonucleotide reductase. Exchange of iron and Mössbauer spectroscopy of the protein B2 subunit of the *Escherichia coli* enzyme. *J. Biol. Chem.* 248:7464–72
105. Mühlenhoff U, Molik S, Godoy JR, Uzarska MA, Richter N, et al. 2010. Cytosolic monothiol glutaredoxins function in intracellular iron sensing and trafficking via their bound iron-sulfur cluster. *Cell Metab*. 12:373–85
106. Sluder IT, Nitika, Knighton LE, Truman AW. 2018. The Hsp70 co-chaperone Ydj1/HDJ2 regulates ribonucleotide reductase activity. *PLOS Genet*. 14:e1007462
107. Zhang Y, Li H, Zhang C, An X, Liu L, et al. 2014. Conserved electron donor complex Dre2-Tah18 is required for ribonucleotide reductase metallocofactor assembly and DNA synthesis. *PNAS* 111:E1695–704
108. Hristova D, Wu CH, Jiang W, Krebs C, Stubbe J. 2008. Importance of the maintenance pathway in the regulation of the activity of *Escherichia coli* ribonucleotide reductase. *Biochemistry* 47:3989–99
109. Ortigosa AD, Hristova D, Perlstein DL, Zhang Z, Huang M, Stubbe J. 2006. Determination of the in vivo stoichiometry of tyrosyl radical per $\beta\beta'$ in *Saccharomyces cerevisiae* ribonucleotide reductase. *Biochemistry* 45:12282–94
110. Lassmann G, Thelander L, Gräslund A. 1992. EPR stopped-flow studies of the reaction of the tyrosyl radical of protein R2 from ribonucleotide reductase with hydroxyurea. *Biochem. Biophys. Res. Commun.* 188:879–87
111. Swarts JC, Aquino MA, Han JY, Lam KY, Sykes AG. 1995. Kinetic studies on the reduction of the tyrosyl radical of the R2 subunit of *E. coli* ribonucleotide reductase. *Biochim. Biophys. Acta Protein Struct. Mol. Enzymol.* 1247:215–24
112. Jiang W, Xie J, Varano PT, Krebs C, Bollinger JM. 2010. Two distinct mechanisms of inactivation of the class Ic ribonucleotide reductase from *Chlamydia trachomatis* by hydroxyurea: implications for the protein gating of intersubunit electron transfer. *Biochemistry* 49:5340–49
113. Karlsson M, Sahlin M, Sjöberg BM. 1992. *Escherichia coli* ribonucleotide reductase. Radical susceptibility to hydroxyurea is dependent on the regulatory state of the enzyme. *J. Biol. Chem.* 267:12622–26
114. Bollinger JM Jr., Jiang W, Green MT, Krebs C. 2008. The manganese(IV)/iron(III) cofactor of *Chlamydia trachomatis* ribonucleotide reductase: structure, assembly, radical initiation, and evolution. *Curr. Opin. Struct. Biol.* 18:650–57

115. Aye Y, Long MJ, Stubbe J. 2012. Mechanistic studies of semicarbazone triapine targeting human ribonucleotide reductase in vitro and in mammalian cells: tyrosyl radical quenching not involving reactive oxygen species. *J. Biol. Chem.* 287:35768–78
116. Popović-Bijelić A, Kowol CR, Lind ME, Luo J, Himo F, et al. 2011. Ribonucleotide reductase inhibition by metal complexes of triapine (3-aminopyridine-2-carboxaldehyde thiosemicarbazone): a combined experimental and theoretical study. *J. Inorg. Biochem.* 105:1422–31
117. Boal AK, Cotruvo JA Jr., Stubbe J, Rosenzweig AC. 2010. Structural basis for activation of class Ib ribonucleotide reductase. *Science* 329:1526–30
118. Parker MJ, Maggiolo AO, Thomas WC, Kim A, Meisburger SP, et al. 2018. An endogenous dAMP ligand in *Bacillus subtilis* class Ib RNR promotes assembly of a noncanonical dimer for regulation by dATP. *PNAS* 115:E4594–603
119. Johansson R, Jonna Venkateswara R, Kumar R, Nayeri N, Lundin D, et al. 2016. Structural mechanism of allosteric activity regulation in a ribonucleotide reductase with double ATP cones. *Structure* 24:906–17

Annual Review of Biochemistry

Volume 89, 2020

Contents

Errata

An online log of corrections to *Annual Review of Biochemistry* articles may be found at http://www.annualreviews.org/errata/biochem